DISSERTATION

Multimodal navigation in deep brain stimulation surgery
Multimodale Navigation in der Tiefenhirnstimulationschirurgie

zur Erlangung des akademischen Grades
Doctor of Philosophy (PhD)

vorgelegt der Medizinischen Fakultät
Charité – Universitätsmedizin Berlin

von
Simón Oxenford

Erstbetreuer: Prof Wolf-Julian Neumann
Datum der Promotion: 29.11.2024

Table of contents

List of figures

List of abbreviations

AD	Alzheimer’s disease
ADNI	Alzheimer's Disease Neuroimaging Initiative
ALIC	anterior limb of the capsula interna
CT	computed tomography
DBS	deep brain stimulation
ET	essential tremor
fMRI	functional magnetic resonance imaging
GPi	internal globus pallidus
HarP	Harmonized Protocol
MER	micro-electrode recordings
MNI	Montreal Neurological Institute ICBM 2009b Nonlinear Asymmetric template
MRI	magnetic resonance imaging
Nacc	nucleus accumbens
NRMS	normalized root mean square
OCD	obsessive compulsive disorder
PD	Parkinson’s disease
RMS	root mean square
SCC	subgenual cingulate cortex
SDK	software development kit
SNR	signal to noise ratio
SPARE-AD	Spatial Pattern of Abnormality for Recognition of Early Alzheimer’s disease
STN	subthalamic nucleus
VIM	ventral intermediate nucleus of the thalamus

Abstract

Electrode implant location in deep brain stimulation (DBS) surgery is defined from multiple sources of information: brain imaging for planning; electrophysiological recordings for basal ganglia nuclei characterization; and test stimulations for intra-operative assessment of physiological and side effects. While each of these steps are established procedures by their own, methods working towards their integration and aggregation lack.

We addressed this topic in a published proof-of-concept toolbox perusing multimodal data processing during DBS surgery. Here, we re-iterate on this theme placing it into a broader context and we introduce novel implementations working towards a robust and reliable software program.

We developed a platform for multimodal data aggregation during DBS surgery and validated it with a cohort of 52 Parkinson's disease DBS patients from our center. We also exemplified the use of one of the platform's modules with a cohort of 118 patients from the Alzheimer's disease neuroimaging initiative database.

The novel platform extends the previously published toolbox including a state-of-the-art electrophysiology acquisition and processing software. We show a general correspondence between imaging and electrophysiological features extracted from DBS surgery. We furthermore present novel biomarkers resulting from the integration of the multiple data sources.

The developed platform for real-time DBS surgery navigation integrates different sources of information into three-dimensional representations of the data—potentially becoming an important element for decision making assistance during DBS surgery.

Zusammenfassung

Die Position der implantierten Elektrode zur tiefen Hirnstimulation (THS) wird anhand mehrerer Informationsquellen bestimmt: Bildgebung des Gehirns für die Planung, elektrophysiologische Aufzeichnungen für die Charakterisierung der Basalganglienkerne und Teststimulationen für die intraoperative Bewertung der physiologischen Auswirkungen und Nebenwirkungen. Während jeder dieser Schritte für sich genommen ein etabliertes Verfahren darstellt, fehlen Methoden, welche auf die Integration und Zusammenführung der Informationsquellen hinarbeiten.

Wir haben uns mit diesem Thema in einer veröffentlichten Proof-of-Concept-Toolbox auseinandergesetzt, welche die multimodale Datenverarbeitung während der THS-Operation untersucht. In der vorliegenden Arbeit greifen wir dieses Thema erneut auf, indem wir es in einen breiteren Kontext stellen und neue Implementierungen vorstellen, die auf ein robustes und zuverlässiges Softwareprogramm hinarbeiten.

Wir haben eine Plattform für die multimodale Datenaggregation während einer THS-Operation entwickelt und sie mit einer Kohorte von 52 Parkinson-Patienten aus unserem Zentrum validiert. Außerdem haben wir die Verwendung eines Moduls der Plattform anhand einer Kohorte von 118 Patienten aus der Neuroimaging-Initiative für die Alzheimer-Krankheit exemplifiziert.

Die neuartige Plattform erweitert die zuvor veröffentlichte Toolbox um eine hochmoderne Software für die elektrophysiologische Erfassung und Verarbeitung. Wir zeigen eine allgemeine Korrelation zwischen bildgebenden und elektrophysiologischen Merkmalen, welche aus der THS-Operation extrahiert wurden. Darüber hinaus stellen wir neue Biomarker vor, die sich aus der Integration der verschiedenen Datenquellen ergeben.

Die entwickelte Plattform für die Echtzeit-Navigation bei THS-Operationen integriert verschiedene Informationsquellen in 3D-Darstellungen der Daten, die zukünftig ein wichtiges Element für die Entscheidungsfindung bei THS-Operationen sein könnten.

1 Introduction

Deep brain stimulation (DBS) surgery is an established procedure to treat Parkinson's disease (PD) symptoms and a growing number of other neurological and psychiatric conditions (A. M. Lozano et al., 2019). The surgery consists of implanting small electrode leads (~1.3 mm diameter) in specific brain regions through which stimulation is delivered. The stimulation protocol (contacts configuration, amplitude, and frequency) is set via the implantable pulse generator—a pacemaker-like device surgically placed in the sub-clavicular area.

The target structures vary according to the condition being treated: the subthalamic nucleus (STN) and internal globus pallidus (GPi) are mainly targeted for PD patients; the ventral intermediate nucleus of the thalamus (VIM) for essential tremor (ET); the anterior limb of the capsula interna (ALIC), nucleus accumbens (NAcc) and STN for obsessive compulsive disorder (OCD); subgenual cingulate cortex (SCC) and NAcc for major depression; and fornix for Alzheimer's disease (AD) (A. M. Lozano et al., 2019).

While historically some of these targets were based on serendipitous discoveries—including DBS for AD, inspired by stimulation induced flashbacks during DBS surgery for obesity (Hamani et al., 2008; for a review see Hariz et al., 2022)—current advances in DBS are fueled by innovations in image processing, electrode design and biomarker detection (Krauss et al., 2021; Schulder et al., 2023).

In particular, by employing processing and simulation techniques, DBS started to be looked at from a computational perspective (Horn, 2019; McIntyre et al., 2004). DBS leads can be reconstructed from post-operative computed tomography (CT) scans (Dembek et al., 2021; Husch et al., 2018) and fused together with anatomically-detailed pre-operative magnetic resonance imaging (MRI). Additionally, electric fields induced by the stimulation can be computationally simulated, estimating the tissue being stimulated (Horn et al., 2017; Kuncel et al., 2008; Mädler and Coenen, 2012). Furthermore, patient images can be fused with average template brains (Ashburner and Friston, 2011; Avants et al., 2008), allowing to analyze and compare a cohort of patients within the same reference system and together with normative data.

There are different methodologies and implementations to calculate the aforementioned features (see for example the citations in the previous paragraph), as well as software

tools that include all these steps as a pipeline for DBS image analysis (D'Albis et al., 2015; Horn et al., 2019; Noecker et al., 2021). Such is the case of Lead-DBS, an open-source Matlab toolbox with advanced image processing capabilities (Horn et al., 2019; Horn and Kühn, 2015; Neudorfer et al., 2023). Lead-DBS has empowered over 500 research publications (https://www.lead-dbs.org/about/publications/), including group studies to explain DBS effects in PD (Horn et al., 2017; Sobesky et al., 2022); ET (Al-Fatly et al., 2019); dystonia (Horn et al., 2022); OCD (Baldermann et al., 2019; Li et al., 2020); and AD (Ríos et al., 2022). These studies build models of DBS, some proposing refined targets and optimal *sweet-spots* which could potentially drive new clinical trials in the future.

In this study we set out to analyze the translation of some of these imaging advances into the surgical realm; and integrate them together with other resources available during surgery, such as pre-operative planning and intra-operative electrophysiology. In the next sections we will introduce the concept of mapping normative data into patient space; the surgical procedure in more detail; and how this work addresses some of the current limitations in these areas.

1.1 Group analysis & image normalization

In the previous section we mentioned the process of fusing different images together—from the same patient across different modalities, or across patients. This is achieved via a method called image registration, in which a moving image is transformed to a fixed image, leading to a transformation linking the two (Avants et al., 2014). Depending on the degrees of freedom it has, the transformation can be linear or non-linear, the latter allowing to locally deform the image and thus achieving better correspondence between images from different brains (Avants et al., 2008).

Normalization is a type of non-linear registration where the moving image is a patient image, and the fixed image is an average reference template brain, such as the Montreal Neurological Institute (MNI) brain, a commonly used template in neuroimaging. While there are different versions of this template, in this work we will use MNI to refer to the ICBM 2009b Nonlinear Asymmetric template (Fonov et al., 2009). By mapping multiple patients to the same space, then the same reference system is used for all of them, allowing to compare between cohorts and centers. In MNI space there are also multiple definition of atlases: structure delineations derived from manual segmentations, or

functional studies, for example. These can then be mapped to patient space, deriving automatic segmentations of structures of interest (i.e., atlas-based, or normalization-based segmentations).

The functional MRI (fMRI) literature has mainly driven the development of the normalization techniques over the years (Jenkinson et al., 2012), and this is now an established process leading to accurate mappings in the cortex (Klein et al., 2009) as well as subcortex (Ewert et al., 2019). While the DBS field also employs this technique, it depends on higher precision: images are generally smoothed with an up to 8 mm kernel after normalization in fMRI whereas a 2 mm difference in DBS electrode placement can separate a good from a poor responder (Horn et al., 2019).

Since in this study we are interested in having an accurate link to patient space, and use this information intra-operatively, we set out to refine this step, and provide a method to manually fix for registrations misalignments. In the methods section we will describe this more in detail.

1.2 Deep brain stimulation surgery

Imaging also plays a huge role during DBS surgery itself (Schulder et al., 2023). MRI scans of the patient's brain are used by surgeons to identify target structures and plan the trajectories for the DBS electrodes (Starr et al., 2002). CT scans—with the stereotactic frame attached to patient's head—allow to translate coordinates from the MRI to the frame's coordinate system. Furthermore, some centers also use intra-operative imaging to confirm electrode placement (Martin et al., 2005).

Apart from employing imaging techniques, intra-operative confirmation can also be achieved via an electrophysiology assessment: previous to the DBS electrode implantation, exploratory micro-electrodes recordings (MER) of brain signals are carried out along the planned trajectory and 2 mm parallel to it, in an orthogonal or 45 degree rotated Ben-gun configuration (Benazzouz et al., 2002). Some nuclei are identifiable by their firing patterns, such as the increased bursting activity of the parkinsonian STN and GPi (Bergman et al., 1994; Miller and DeLong, 1988), and are thus recognizable by the surgical team. Leveraging upon this, commercial acquisition systems started to include automatic algorithms to detect such features giving an estimate of the nuclei along the trajectory (Thompson et al., 2018). Additionally, electrophysiology recordings are

commonly followed by test stimulations to assess physiological and side effects. Usually done in one or two coordinates along the trajectory, these stimulations help to better characterize the patient's condition and response to the treatment.

The electrophysiological assessment is not an established procedure in every DBS center given that including this step can lead to longer surgeries and hemorrhagic complications, compared against an imaging alone approach (Zrinzo et al., 2012). Still, patient improvement is comparable between the two (Gadot et al., 2022; Lee et al., 2022; Vinke et al., 2022), and some centers also report the advantages of MER, as for example suggesting a beneficial alternate trajectory in 20% of surgeries (C. S. Lozano et al., 2019).

Finally, the original target position defined from imaging is redefined based on the recordings and intraoperative stimulation assessment, which might suggest a new height along the trajectory and/or an alternative trajectory.

1.3 Challenges

While current practice has shown to be effective, there are still gaps that could be filled to improve the procedure: as mentioned in the last section, imaging and electrophysiology—two processing streams that define the electrode position—are analyzed separately, across different stages of the surgery, missing out on potential benefits of their combination. Additionally, while the MER take place, the electrophysiologist doesn't have a real-time spatial representation of their location. Such feature could be helpful to better understand the signals by putting them into anatomical context, as shown by (Krüger et al., 2020). In this regard, this dissertation focuses on the integration of imaging and electrophysiology, processing raw data to gather relevant information creating anatomically-detailed patient-specific representations of the ongoing state of the surgery. We have started working in this endeavor previously (Oxenford et al., 2022) and we here re-iterate on this theme and scientific focus, putting the work into a broader perspective and improving the implementation of our methods.

From the imaging side, as mentioned in 1.1, we are interested in incorporating patient specific anatomical models as well as high-resolution resources that could put patient images into more context. Thus, the link between patient and template space is of utmost importance but challenged by individual brain anatomy and suboptimal normalization

algorithms. Here we set out to develop methods to refine the normalization output and manually correct mismatches from the process.

From the electrophysiology side, we aim to derive real-time feature extraction to aid surgical procedure. While previous work has demonstrated feasibility of the implementation of real-time algorithms (Khosravi et al., 2020; Valsky et al., 2020), there is a lack in open-source platforms to test, reproduce and benchmark results from different studies.

In this work, to provide an implementation of the methods presented, we build on top of already established platforms and methods, which offer a starting point for our research. The choice of platforms to build upon depends on their reliability, extensibility and real-time performance. In the next section we go over three platforms which have become an essential part of this project.

1.4 Platforms

1.4.1 Lead-DBS (https://www.lead-dbs.org/)

Lead-DBS (Horn et al., 2019; Horn and Kühn, 2015; Neudorfer et al., 2023), already mentioned in previous sections, is a Matlab toolbox for post-operative DBS electrode reconstruction and image processing pipeline for group studies (Treu et al., 2020). We leverage upon the advanced normalization routines developed for basal ganglia (Ewert et al., 2019), as well as high resolution resources, such as DISTAL atlas (Ewert et al., 2017) and post-mortem high-resolution 7T template (Edlow et al., 2019).

1.4.2 3D Slicer (https://www.slicer.org/)

3D Slicer (Slicer; Fedorov et al., 2012; Kikinis et al., 2014) is a general-purpose open-source medical imaging processing and visualization platform. It is built on top of the Insight Toolkit (https://itk.org/) and the Visualization Toolkit (https://vtk.org/), which are industry standard libraries for medical image processing and computer vision. Slicer is used for real-time applications (Ungi et al., 2016), built using a modular approach, and maintained and developed by an active community of researches and industry partners (Kapur et al., 2016).

1.4.3 Open Ephys (https://open-ephys.org/)

Open Ephys (Siegle et al., 2017) is an open-source software for electrophysiology data acquisition and real-time analysis. It shares some of the same principles as Slicer: provides a modular architecture, the possibility to extend functionality by means of custom plug-ins, and an active community. It is used for real-time and closed-loop applications (Dutta et al., 2018), constituting a suitable candidate for handling the electrophysiology component of our platform.

1.5 Summary

We described DBS surgery, and how multiple sources of information—particularly imaging and electrophysiology—are involved in the definition of the electrode implant location. Here we will study whether the two are congruent with each other, and with patient outcome. We further investigate methods for combining the two, and what novel biomarkers can be derived from their integration. To achieve these aims we also develop custom methods for real-time analysis and visualization, building on top of established platforms for imaging and electrophysiology processing.

2 Methods

A central part of this work has been to develop methods needed to investigate the topics of our research. This has been in the form of contribution to the platforms mentioned in the introduction, but also in extending their functionality to meet the needs of the project. In this section we will give an overview of the methods implementation, together with a description of the patient cohorts and analysis done to study DBS from a multi-modal perspective.

2.1 Refining image normalization: WarpDrive

WarpDrive is a toolbox to correct for mismatches after image normalization. It exposes different tools for the user to interact with the normalized image, visualizing it with respect to template data and atlases. This way, the user can visualize specific regions of interest and assess the quality of the correspondence of the images. When recognizing mismatches, the user can place source and target points (then fed into an algorithm that corresponds them) in different ways: it is possible to manually select source and target fiducials; to draw structure delineations matching them to atlases; or to drag and displace regions of interest. We refer to the online documentation for more detailed description of how the tools work (https://github.com/netstim/SlicerNetstim).

WarpDrive is a key component of this project, as it enables an accurate link between patient space and template space. Still, the tool is not restricted to patient-to-template mapping, but is rather built to handle any imaging data. It is included as a module in Slicer, and is also seemlesly integrated with Lead-DBS as a next optional step after image normalization.

2.2 Alzheimer's Disease Neuroimaging Initiative (ADNI) cohort

To exemplify the limitations of normalization algorithms and the usage of WarpDrive, we retrieved a set of patients from the Alzheimer's Disease Neuroimaging Initiative (ADNI) database (adni.loni.usc.edu) and analyzed them comparing manual versus automatic segmentations in relation to brain atrophy.

The selected cohort consisted of 118 patients (56 females; mean age: 75 ± 7.8 years) which included both *Harmonized Protocol* (HarP) manual hippocampus segmentations

(Boccardi et al., 2015a) and the *Spatial Pattern of Abnormality for Recognition of Early Alzheimer's disease* (SPARE-AD) index (Davatzikos et al., 2009). HarP provides consistent patient specific (Boccardi et al., 2015b) and MNI (Wolf et al., 2017) segmentations of the hippocampus. Thus, transforming the MNI segmentation to patient space will lead a good estimate of the accuracy of this atlas-based segmentation. Here we set out to see whether the accuracy of the atlas-based segmentations is associated with brain atrophy (as measured by the SPARE-AD index, which provides a measure of brain atrophy patterns common in AD). Next, we take a set of strongly atrophied brains to showcase how WarpDrive can help improve the accuracy of the registration. Initial transformations were calculated by importing the cohort in Lead-DBS and running normalization with default parameters.

2.3 Multimodal deep brain stimulation surgery navigation: Lead-OR

The Lead-OR project is about integrating, visualizing, and analyzing multiple modalities in real-time during DBS surgery. The spatial correspondence of the data is of utmost importance in this application to provide a starting point for further analysis. In the previous section we described WarpDrive, a tool involved with achieving an accurate mapping from template to native space, allowing to translate high-resolution data (such as atlases) into patient specific space. We will next describe how other resources are also put together in the same space; and then the possibilities that this opens up for processing and analysis.

2.3.1 Import different planning information

DBS surgery implant trajectories can be defined from entry and target points in the patient's reference image. This translates to the stereotactic frame's settings: target X, Y, Z coordinates, and ring and arc angles. Both the patient's image and the frame represent a coordinate system that must be matched to integrate data from them. The correspondence can be achieved by a linear transform computed via fiducial registration between same points defined in both coordinate systems.

To correspond a single trajectory, only two points are needed: target and entry. However, this doesn't fully represent the correspondence in three-dimensional space, one parameter is rather missing: the rotation around this target-entry axis. This information is

important when using multiple micro-electrodes with a Ben-Gun configuration, as their position in space depends on it.

The mapping of the patient's image to the frame and its computation is usually hidden in commercial planning platforms. Still, it is possible to recreate this transform from exported information from the software. Here, we have incorporated two import routines for different platforms, and a plug-in like architecture to further include more in the future.

In Elements Stereotaxy (Brainlab AG, Munich, Germany) the entry and target coordinates (as well as the AC, PC and MS points) are specified in both patient and frame's reference within the planning export file. This allows to match both spaces via fiducial registration thus recreating the rotation around the trajectory's axis.

The ROSA robot (Zimmer Biomet Holdings, Inc., Warsaw, Indiana, U.S.) also exports entry, target, AC, PC and MS in patient space, but not in frame space. Therefore, the rotation around the trajectory axis is not defined.

For both planning software we implemented an import routine to represent the trajectory information in Slicer. This is built as a module which can also visualize and modify planning information featuring two ways of setting the trajectory: from target, ring angle and arc angle; and from target, entry and roll angle (rotation around the axis).

2.3.2 Slicer reference

The planning information is imported and the trajectories are defined to match the frame reference system. To simplify things, the frame's center is set to match Slicer's World center, with a linear transformation defining the transform of coordinates between the two.

In the case where the frame information is not known (such as the case for ROSA), the patient images are AC-PC transformed recreating the same visualization as planning software.

Up to here we described the handling of the imaging data for DBS surgery. Specifically, how Lead-OR recreates the planning information as they were defined in (different) planning software. Additionally, how to accurately represent atlas data, such as structures delineations, in patient specific space. In the following sections we will describe the electrophysiology processing and how it is also mapped to the same space in real-time.

2.3.3 Electrophysiology acquisition and processing

Part of this project, and novel to this dissertation publication, was the development of different plug-ins for the Open Ephys platform. The first one is the NeuroOmega acquisition module, which connects to the NeuroOmega device (Alpha Omega Engineering, Israel) via AlphaOmega's Software Developments Kit (SDK) and queries real-time electrophysiology signals together with the micro-electrode distance to the target value. After the device is connected the user can select from the different available data sources (raw micro-electrode recordings, local field potentials, and macro-electrode recordings, among others). Once enabled, this stream will be sent through the Open Ephys pipeline.

Taking advantage of the modular architecture of Open Ephys, once these signals are streamed into the platform, it is possible to build a processing pipeline from any of the modules available. For example, some built-in modules already provide capabilities for visualization, bandpass filtering, recording, and spike detection.

Further capabilities can also be implemented via custom plugins, as is the case of another module we developed for root mean square (RMS) calculation. This process executes in real-time calculating RMS from data taking a specified time window.

2.3.4 OpenEphys – 3D Slicer communication

The communication between Open Ephys and Slicer is done via the OpenIGTLink library (Tokuda et al., 2009), which specifies a network protocol capable to send transforms, images, and strings, among other data types. We built an Open Ephys plugin that sends the extracted features along each trajectory to Slicer together with the real-time position of the micro-drive.

With the trajectory definition, Ben-Gun configuration, and distance to the target value, the electrophysiological recording sites can be mapped to three-dimensional space (Figure 1). Then, the different features can be represented as different properties in space, such as a tube varying its diameter and color according to the feature's magnitude. This leads to having all multimodal data accurately represented in space in real-time during surgery.

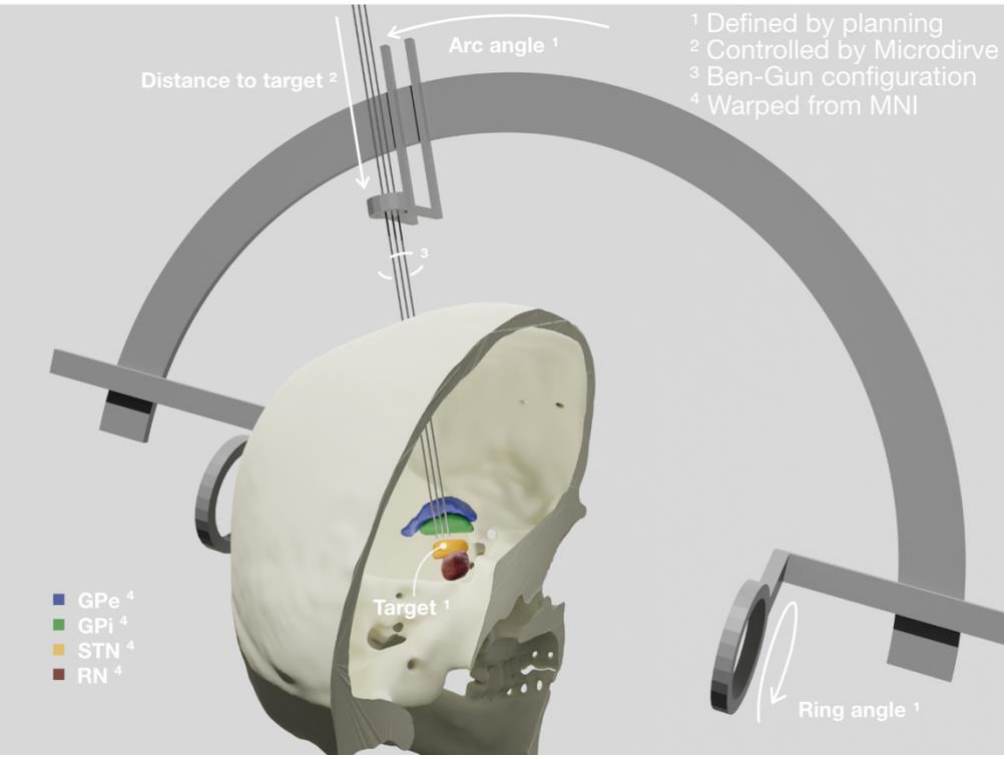

Figure 1. Multiple sources of information to recreate the spatial representation of deep brain stimulation (DBS) surgery. First, planning defines target coordinates, as well as ring and arc angles, describing the trajectory of implantation. The microdrive sets the position of the micro-electrodes along this trajectory. Then, using different Ben-Gun configurations the alternate trajectories are set in space. Nuclei of interest are put together in patient space by transforming atlases from MNI after image normalization. From (Oxenford et al., 2022), used under CC BY 4.0.

2.4 Subthalamic nucleus deep brain stimulation (STN-DBS) patient cohort

To validate this method and further analyze the potentials of multi-modal data aggregation we analyzed a retrospective cohort of patients who underwent DBS surgery at our center between 2017 and 2021. Patient inclusion criteria was based on having complete set of data (pre-operative imaging, Brainlab planning and micro electrode recordings). The cohort was composed of 52 patients, of which 12 females, with a mean age of 61 +/- 9.

Data were visually inspected, discarding trajectories featuring low signal to noise ratio (SNR) or artifacts in the micro-electrode recordings and low SNR or movement artifacts in the imaging. Finally, 236 surgical trajectories were analyzed, from 56 hemispheres of 32 patients.

2.5 Surgical procedure

Patients underwent DBS targeting the STN with an initial imaging-based planning made in Stereotaxy Elements (Brainlab AG, Much, Germany). Depending on the clinical decision for each patient, surgery was done awake or under general anesthesia, with micro-electrode assessment carried out in both cases. Neuroprobe Sonus non-shielded micro-electrodes (Alpha Omega Engineering, Israel) were descended in parallel trajectories probing the surroundings of the target, with 2 to 5 trajectories in an orthogonal or 45-degree rotated Ben-Gun configuration. MER started from 10 mm above the target and finished 4 mm below, in steps of 0.2 to 0.5 mm. After the recordings, test stimulations were carried out, at the target site and 3 mm above, in 0.5 mA steps until recognizing permanent side effects. Finally, based on planning and electrophysiological evaluation, implant location of DBS electrode was determined.

2.6 Offline analysis

We analyzed this patient cohort offline, processing it as the real-time application would. From the imaging side, pre-operative images were co-registered and normalized to MNI space using default settings in Lead-DBS and employing WarpDrive to correct for small mismatches in the alignment, if needed. Implant trajectories were extracted from Brainlab planning, obtaining a patient specific coordinate for each of the recording sites. Then, transforming the DISTAL atlas to patient space, we derived entry and exit points to the STN for each trajectory.

MER were processed to extract their normalized root mean square (NRMS) values: RMS was taken for each of the recording sites and normalized by the median of the first five recordings for each trajectory, as done in previous studies (Zaidel et al., 2009). The choice of this feature was based on taking a commonly used measure in the field and an established straightforward proxy of brain activity (Khosravi et al., 2020; Koirala et al., 2020; Valsky et al., 2020, 2017; Zaidel et al., 2010, 2009). Further features can be extracted and analyzed, including spike analysis as in (Oxenford et al., 2022), and via custom processing pipelines in Open Ephys for the real-time application.

The recordings sites' distance to the target values were normalized across trajectories taking as target a reference point inside the STN (i.e., Caire et al., 2013), thus deriving a normalized distance to target axis to compare all trajectories.

Taking the entry and exit sites from imaging, and the NRMS measure from electrophysiology, we analyzed whether the trajectories definition of the STN agreed from both perspectives. For this, we compared the trajectories based on their vicinity to the STN and analyzed if the difference in NRMS activity matched the STN entry and exit sites.

2.7 Active contacts location

Based on post-operative scans and clinical stimulation settings we obtained the coordinates of the active contacts location after reconstructing the DBS electrodes as implemented in Lead-DBS. We then mapped this location to the nearest coordinate along the patient's trajectories as an additional verification step of the agreement of the different modalities.

2.8 Brain-shift analysis

We carried out an additional analysis estimating brain-shift, using an imaging-approach and an electrophysiology-approach, and comparing the two.

The brain-shift imaging-estimate was defined using pre- and post-operative imaging, as implemented in Lead-DBS: post-operative images were co-registered to the pre-operative imaging, first using the whole brain and then locally, focusing on the basal ganglia. The resulting transformation was used to transform coordinates along the trajectories. We defined the brain-shift imaging-estimate as the resulting displacement.

The brain-shift electrophysiology-estimate was defined using MER features and their correspondence to the atlas-based definition of the STN. The NRMS trace for each trajectory was cross correlated with its spatial vicinity to the STN. This resulted in a xcorr value and a lag value; the lag representing the displacement of the NRMS trace to maximally overlap with the STN. We defined the brain-shift electrophysiology-estimate as the lag resulting from this computation.

Performing a correlation analysis we calculated the association between the two measures of brain-shift. This is a preliminary evaluation to assess the potential of this biomarker as a real-time estimate of brain-shift during surgery.

3 Results

A central component of the results of this dissertation work come in the form of software plug-ins for multimodal data analysis and visualization during DBS surgery. These modules encompass the Lead-OR project (figure 2) and form a platform which can be customized and further extended to build real-time processing pipelines enabling novel types of analysis to create informative representations of the ongoing state of the surgery.

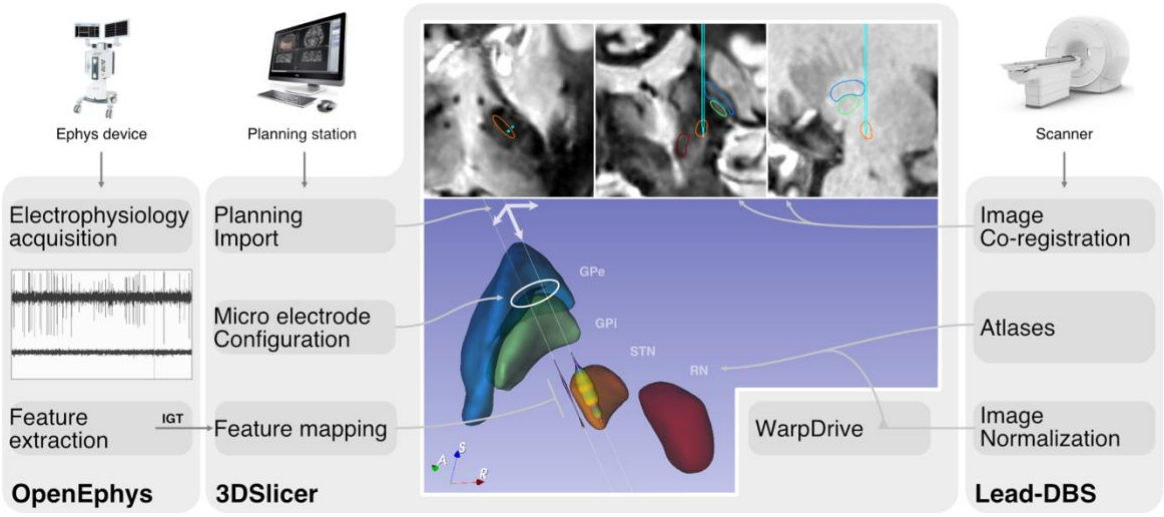

Figure 2. Overview of the Lead-OR project implementation. The Open Ephys platform connects to the electrophysiology acquisition device (in this project the NeuroOmega from Alpha Omega), visualizes and processes the incoming signals extracting features of interest. Features are sent to 3D Slicer via OpenIGTLink (IGT) and are mapped to their spatial location defined by the planning, microelectrode configuration, and distance to target. Here, the normalized root mean square value of the signals is informing the diameter and color of a tube along the trajectories. Currently, planning information can be imported from Brainlab and ROSA stations, with the possibility to extend to more platforms. Patient images are co-registered and visualized with in-plane slices defined by the planned trajectory. After image normalization in Lead-DBS, atlases can be transformed into patient space, deriving an atlas-based segmentation which can be further refined using WarpDrive. This way, the multiple modalities and sources of information are spatially corresponded and displayed to create a meaningful representation of the ongoing state of deep brain stimulation surgery. GPe: external globus pallidus; GPi: internal globus pallidus; STN: subthalamic nucleus; RN: red nucleus.

3.1 Novel tools implementation

The implementations built around this work allow: connecting and streaming data from the NeuroOmega device to the OpenEphys GUI; extracting electrophysiological features in real-time; importing of stereotactic surgery planning; refining atlas-based

segmentations via manual interactions; and visualizing in real-time imaging, together with high resolution data resources and electrophysiology features in patient specific space, representing the state of DBS surgery. An overview of the tools and their interplay is presented in figure 2.

3.2 Increasing brain atrophy challenges automatic registrations

Automatic atlas-based segmentation can be challenging in cases with abnormal brain anatomy, such as atrophy. The accuracy of HarP hipocampus atlas-based segmentations and brain atrophy patterns measured by SPARE-AD present a significant relation in a set of ADNI patients featuring both data (Pearson $R = -0.57$; $p < 1e-10$; Figure 3). Manually refining the transformations in WarpDrive improves the accuracy of the atlas-based segmentations, deriving a more precise link to MNI space.

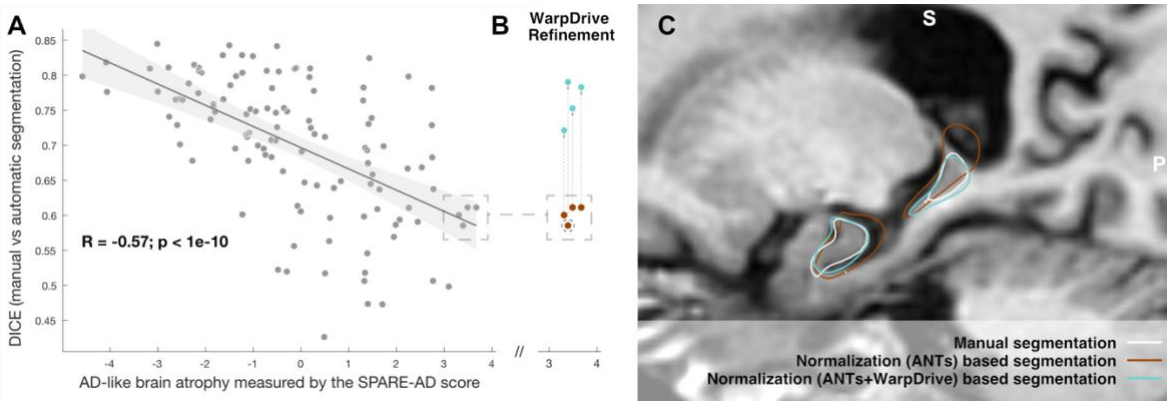

Figure 3. Accuracy of automatic registrations is challenged by brain atrophy. Panel A shows the association (Pearson $R = -0.57$; $p < 1e-10$) between the accuracy of atlas-based segmentations (as measured by the DICE score between manual and MNI-transformed segmentations) and brain atrophy (as measured by the SPARE-AD score). Cases with strong atrophy are tough for automatic algorithms and candidates to be improved by manual refinements in WarpDrive (B). One example case is illustrated in C, showing the manual, automatic, and refined segmentations of the hippocampus (note that the user was blinded to the manual segmentation while doing the refinements).

3.3 Overall agreement between imaging and electrophysiology

As a validation of the Lead-OR platform, a general correspondence between electrophysiology derived features and imaging is seen. Normalized root mean square values along the trajectories depict a region with higher activity that lays within the imaging-defined STN boundaries (figure 4).

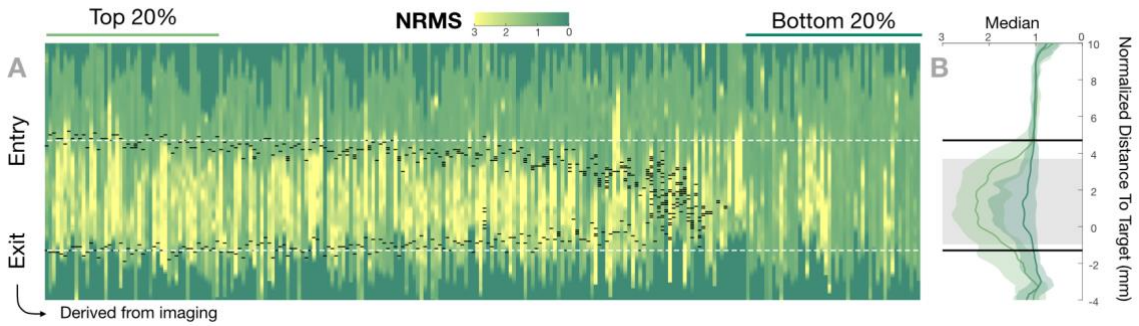

Figure 4. Agreement between electrophysiology and imaging. In panel A, each vertical line represents a trajectory from left to right according to their distance to the subthalamic nucleus (STN). The color indicates the normalized root mean square (NRMS) value derived from the electrophysiology signals and the black dashed lines represent the entry and exit sites to the STN as defined from the imaging. In Panel B we take the top 20% trajectories and compare the median NRMS along the trajectories against the bottom 20%. A significantly different portion of the two electrophysiology derived features (nonparametric Wilcoxon's signed-rank test $p < 0.01$ with false discovery rate correction) coincides with the entry and exit sites of the imaging derived STN. From (Oxenford et al., 2022), used under CC BY 4.0, cropped from original.

3.4 Active contact locations match expected imaging and electrophysiology sites

The clinical stimulation settings of the patients mapped to the surgical trajectories present a correspondence with electrophysiological and imaging features (figure 5).

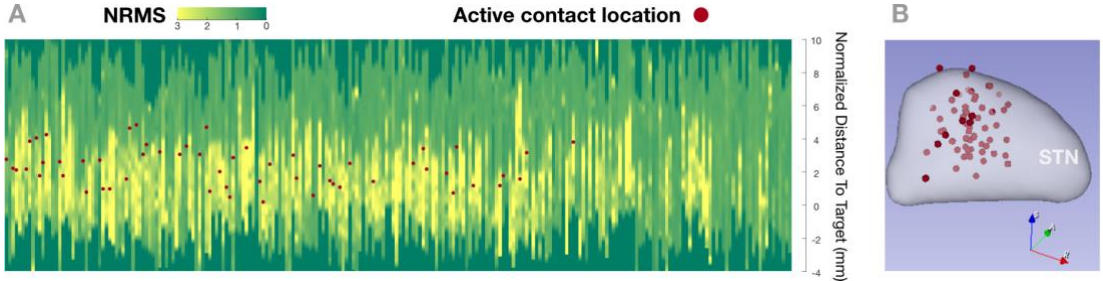

Figure 5. Deep brain stimulation (DBS) electrodes active contact location. The figure visually illustrates the location of the DBS active contacts with respect to the trajectory normalized root mean square (NRMS) traces (A) and the subthalamic nucleus (STN) in MNI space (B). This serves as a further confirmation step of the alignment of the multiple modalities involved in DBS surgery. From (Oxenford et al., 2022), used under CC BY 4.0, cropped from original.

3.5 Intra-operative electrophysiology-based and post-operative imaging-based measures of brain-shift are associated

Although a general correspondence is seen, it is the discrepancy between the imaging and electrophysiology that also inform about new insights. The cross-correlation lag

describing this disagreement was taken as an estimate of intra-operative brain-shift measure and compared against an imaging-based post-operative brain-shift estimate. The data present an association between the two (figure 6) constituting a new biomarker for brain-shift detection in real-time during surgery.

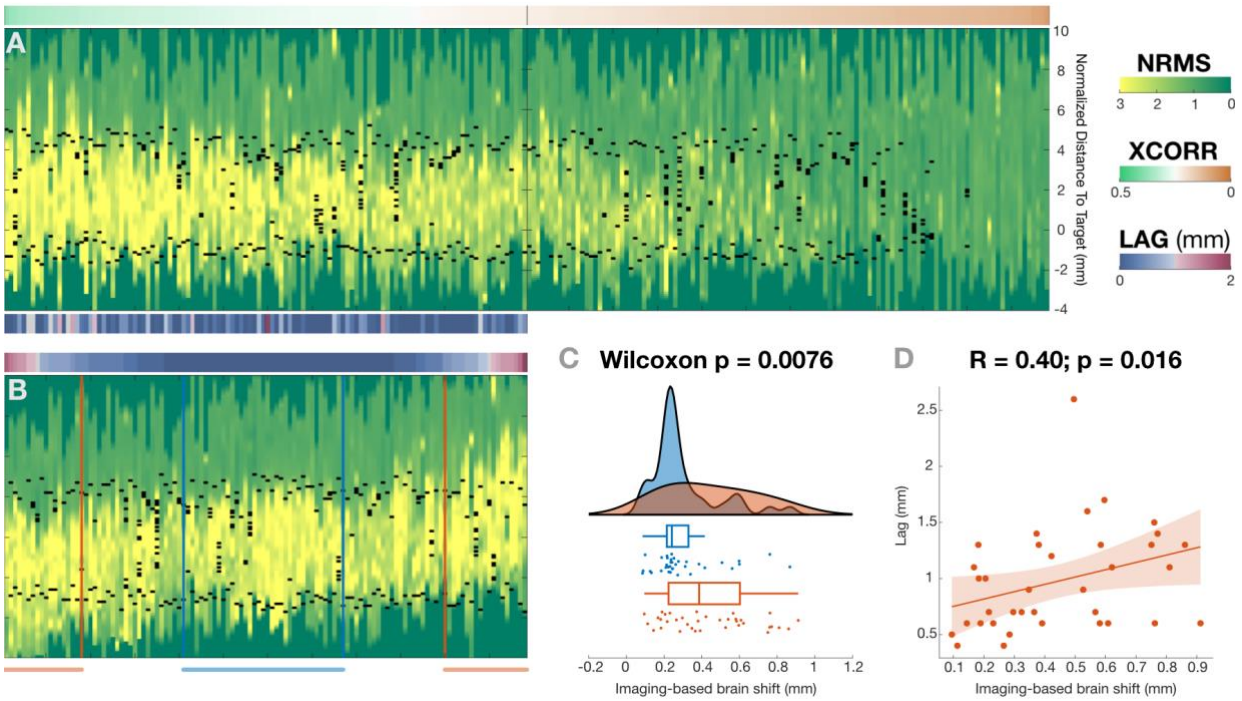

Figure 6. Brain-shift analysis. This figure illustrates the analysis and results derived from the brain-shift processing pipeline. Panel A shows the normalized root mean square (NRMS) traces and subthalamic nucleus (STN) entry and exit for each trajectory. The NRMS traces and the imaging defined STN were cross-correlated, deriving a correlation value (xcorr) and a lag value, which defines the lag at which the maximum xcorr is reached. In panels A and B, the trajectory traces are sorted according to the xcorr and lag values, respectively. Panel B contains the top half of the trajectories: trajectories that intersect the STN from the imaging side and that show electrophysiology activity measured by the NRMS. Next, the no-lag versus high-lag (values above 1 standard deviation) trajectories are compared. In C, the two groups have different distribution of the imaging-based brain-shift value (Wilcoxon's signed-rank test $p = 0.0076$). In D, the lag of the high-lag trajectories (representing the electrophysiology-derived brain-shift) is significantly associated with the post-operative imaging-based brain-shift (Spearman $R = 0.40,\ p = 0.016$). From (Oxenford et al., 2022), used under CC BY 4.0, modified from original.

4 Discussion

4.1 Short summary of results

We developed and validated of a platform combining several methods for the analysis and real-time visualization of DBS surgery.

These include:

- Providing an accurate link between patient and template space, via manual refinements of image normalization.
- Importing of several commercial planning systems into a common framework for further analysis and visualization.
- Acquiring NeuroOmega signals through a plugin into a state-of-the-art electrophysiology processing platform.
- Integrating all the above, with real-time processing and visualization of micro-electrode recordings together patient specific imaging and high-resolution resources.
- Exploring new avenues for biomarker detection relevant for DBS surgery from a multi-modal perspective, including estimating brain-shift based on intra-operative micro-electrode recordings and pre-operative imaging.

Our results suggest that the integration of multiple data sources is not only possible, but that it can be leveraged upon to provide novel insights from DBS surgery. A significant development work was needed to carry out the aims of this study, from achieving real-time signal acquisition and processing, to precisely correspond high resolution imaging resources together. While highly methodological, in this work we also present how novel scientific questions can arise from the methods and, following this direction, we set out to study the integration of multiple data as a biomarker for brain-shift during surgery.

4.2 Embedding the results into the current state of research

This work intends to fill a gap in the current methodology practice and bridge different areas of research within the DBS field, including electrophysiology and imaging. From the electrophysiology side, for example, there has been advances in feature extraction from MER recordings (Koirala et al., 2020; Valsky et al., 2017; Zaidel et al., 2010, 2009),

including real-time machine learning approaches (Valsky et al., 2020), and even nowadays incorporated into commercially available systems (Thompson et al., 2018). The imaging field, on the other hand, has also seen advanced with respect with high(-er) resolution imaging for clinical use (Forstmann et al., 2017; Tao et al., 2023) and for template creation (Amunts et al., 2013; Edlow et al., 2019). While DBS image-guided surgery navigation started to be studied (Krüger et al., 2020), its integration with electrophysiology and additional resources available during surgery is still underexplored.

Here, we bring these different components together into one common platform for real-time electrophysiology and imaging processing and visualization. This way we intend to leverage upon, and not disregard, the multiple sources of information available during surgery. We present a platform to integrate imaging and electrophysiology together, building on top of established software for image navigated surgery and real-time electrophysiology acquisition and analysis. We take advantage of high-quality building components and extend them to meet the needs of this application.

The toolbox provides a new way of processing and visualizing data, and our results present how this novel fusion paradigm can be used to derive biomarkers for DBS surgery. In particular, we present a real-time brain-shift estimation algorithm that could potentially be of assistance during surgery. Like this, we envision further developments in this realm that will open up from multi-modal data aggregation, some of which we introduce in the next section.

4.3 Implications for practice and future research

This study has several implications regarding current practice and future research directions. We present a platform that allows for new types of analysis and opens new avenues for research and clinical applications. The tools developed here could become part of a decision-making assistance application in the operation room, providing insights regarding current state of surgery. For surgeons and neurophysiologists in training, this platform presents educational value, since it brings together all different modalities involved in the surgery into one visualization. This can be an easy-to-grasp representation of the planning, micro-electrodes disposition and patient anatomy that current commercial software do not provide.

There are several future research possibilities starting from this work that we foresee taking the imaging and electrophysiology integration and further investigating it with new research questions in mind.

Such is the case, first, of mapping the intra-operative stimulation testing to anatomical space. These data, together with patient assessment and/or electromyography from muscles, could be used to inform what target structures and fiber-tracts are associated with specific side effects, for example. It could also be used as a dataset to validate novel stimulation modeling algorithms, which could evolve into predictive methods to integrate within Lead-OR. While we started to look at these data (figure 7), further work is needed to formally analyze it and derive conclusions from.

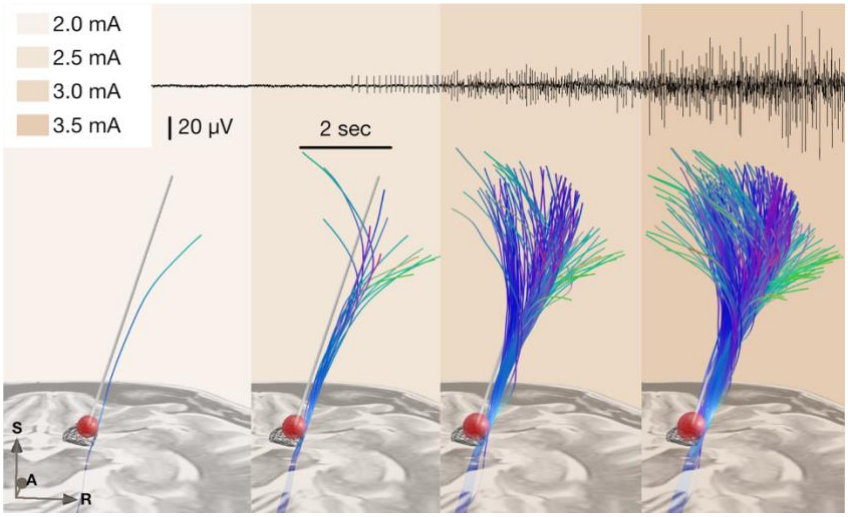

Figure 7. Lead-OR integration with stimulation data. The figure shows an example electromyography trace recorded from the brachioradialis muscle, as the stimulation assessment during deep brain stimulation (DBS) surgery was being done (colors in the figure indicate increasing stimulation amplitude). The bottom panel shows the Lead-OR visualization of the stimulation site with respect with the imaging and together with internal capsule fiber-tracts from a high resolution atlas (Petersen et al., 2019) transformed into patient specific space. Only fiber-tracts that intersect a simulated volume of tissue activated (derived similarly to Dembek et al., 2017) are displayed in each step. This exemplary figure that integrates imaging and stimulation is a preface to future work that could more extensively analyze these kinds of data. From (Oxenford et al., 2022), used under CC BY 4.0.

Second, by further developing MER processing algorithms, like extracting specific frequency-band activity or spikes, an electrophysiological characterization of the basal ganglia region can be developed. Once a reliable map is generated from multiple surgical data, then the real-time application could compare against this map to further inform the intraoperative assessment of the surgery. We also envision the application of Lead-OR

as a platform to benchmark and test different MER processing algorithms promoting open-science practices.

Third, with further advances in VR/AR technologies and taking advantage of good quality open-source solutions (for example 3D Slicer has extensions for VR applications; Choueib et al., 2019), the 3D visualization could be further explored in a more immersive way. The potential for this is more evident for the pre-operative stage, where multiple patient and high-resolution data could be visualized for refining the surgery planning. Such applications are already being developed (Noecker et al., 2023).

Finally, we also extend on the field of image registration, in particular image normalization, where there is a growing interest in fusing multiple-modality and high-resolution data. With WarpDrive having a general implementation and not being restricted to specific DBS cases, we envision the tool having growing impact in this area. For example, it could be used to improve normalization in histology to MRI (Adler et al., 2014; Iglesias et al., 2018), or in specific regions of interest, like the case of sub-field fMRI (Bandettini et al., 2021).

4.4 Limitations

Although we count with high quality data, there were still some cases where data were contaminated with artifacts common to clinical practice: patient movements during imaging, mixt MER step acquisition, and variable depth of anesthesia. Also, given that the data were acquired retrospectively, not every acquisition parameter of the imaging and electrophysiology was controlled for. These factors can make the data heterogenous, and we therefore performed (pre-) processing steps to normalize it and correct for artifacts. Still some cases had to be discarded before further processing, since they didn’t provide sufficient signal to noise ratio for the analysis.

Additionally, other limitations come in the form of processing methods themselves. Image normalization used for aggregating multiple imaging data still has some suboptimal results for some applications—especially when the aim is to achieve high accuracy in rather small regions of interest. To address this, we based our analysis on previously published registration routines (Ewert et al., 2019) and built WarpDrive on top of that. However, we do not intend for WarpDrive to be the ultimate solution in every scenario. The tool still relies on the user having neuroanatomical knowledge and sufficiently detailed images to visualize the areas of interest. Since it depends on the user, the

process becomes less objective, which might seem counterintuitive. However, the subjectivity can bring additional refinements adding value to the data that would otherwise stay unexploited during the analysis.

From the electrophysiology processing side there are different artifacts of the signals arising from the nature of the recording that are cumbersome to avoid and can thus contaminate the data. Cardioballistic artifacts enter this categorization, as well as the signal amplitude attenuation following the tissue displacements caused by the electrode descend. Still, data were a sufficient resource for the aims of this study, which were not to dive deep into electrophysiological details, but rather propose first steps towards a new way of processing and navigating data.

Finally, throughout this study we mentioned the use of normative and atlas data, and we used these resources for our work. While having a common reference for the analysis allows for different examinations of the data, this takes it out of its native space, which still remains the gold standard for patient specific analysis. Additionally, the use of atlases defined in template space also come with the limitations of how they were conceptualized, acquired and built. We here took special attention when linking patient and template spaces (e.g., by including the WarpDrive tool) which helped bringing this work together.

5 Conclusions

Within this work we provide a new framework for multi-modal data aggregation for DBS surgery. We build upon a previously published toolbox and further extend the platform for improved real-time performance and additional electrophysiology processing capabilities. We validate the platform based on retrospective cohorts and show potential avenues for future research including a novel biomarker that informs the brain-shift occurring during surgery. This translational work has direct applications in DBS surgery and could become a source of valuable insights during decision making—potentially improving patient outcome after surgery.

Reference list

Adler, D.H., Pluta, J., Kadivar, S., Craige, C., Gee, J.C., Avants, B.B., Yushkevich, P.A., 2014. Histology-derived volumetric annotation of the human hippocampal subfields in postmortem MRI 84, 505–523. https://doi.org/10.1016/j.neuroimage.2013.08.067

Al-Fatly, B., Ewert, S., Kübler, D., Kroneberg, D., Horn, A., Kühn, A.A., 2019. Connectivity profile of thalamic deep brain stimulation to effectively treat essential tremor. Brain. https://doi.org/10.1093/brain/awz236

Amunts, K., Lepage, C., Borgeat, L., Mohlberg, H., Dickscheid, T., Rousseau, M.E., Bludau, S., Bazin, P.L., Lewis, L.B., Oros-Peusquens, A.M., Shah, N.J., Lippert, T., Zilles, K., Evans, A.C., 2013. BigBrain: An Ultrahigh-Resolution 3D Human Brain Model. Science 340, 1472–1475. https://doi.org/10.1126/science.1235381

Ashburner, J., Friston, K.J., 2011. Diffeomorphic registration using geodesic shooting and Gauss–Newton optimisation. NeuroImage 55, 954–967. https://doi.org/10.1016/j.neuroimage.2010.12.049

Avants, B.B., Epstein, C.L., Grossman, M., Gee, J.C., 2008. Symmetric diffeomorphic image registration with cross-correlation: Evaluating automated labeling of elderly and neurodegenerative brain. Med. Image Anal., Special Issue on The Third International Workshop on Biomedical Image Registration – WBIR 2006 12, 26–41. https://doi.org/10.1016/j.media.2007.06.004

Avants, B.B., Tustison, N.J., Stauffer, M., Song, G., Wu, B., Gee, J.C., 2014. The Insight ToolKit image registration framework. Front. Neuroinformatics 8.

Baldermann, J.C., Melzer, C., Zapf, A., Kohl, S., Timmermann, L., Tittgemeyer, M., Huys, D., Visser-Vandewalle, V., Kühn, A.A., Horn, A., Kuhn, J., 2019. Connectivity Profile Predictive of Effective Deep Brain Stimulation in Obsessive-Compulsive Disorder. Biol. Psychiatry 85, 735–743. https://doi.org/10.1016/j.biopsych.2018.12.019

Bandettini, P.A., Huber, L., Finn, E.S., 2021. Challenges and opportunities of mesoscopic brain mapping with fMRI. Curr. Opin. Behav. Sci., Deep Imaging - Personalized Neuroscience 40, 189–200. https://doi.org/10.1016/j.cobeha.2021.06.002

Benazzouz, A., Breit, S., Koudsie, A., Pollak, P., Krack, P., Benabid, A.-L., 2002. Intraoperative microrecordings of the subthalamic nucleus in Parkinson's disease. Mov. Disord. 17, S145–S149. https://doi.org/10.1002/mds.10156

Bergman, H., Wichmann, T., Karmon, B., DeLong, M.R., 1994. The primate subthalamic nucleus. II. Neuronal activity in the MPTP model of parkinsonism. J. Neurophysiol. 72, 507–520. https://doi.org/10.1152/jn.1994.72.2.507

Boccardi, M., Bocchetta, M., Apostolova, L.G., Barnes, J., Bartzokis, G., Corbetta, G., DeCarli, C., deToledo-Morrell, L., Firbank, M., Ganzola, R., Gerritsen, L., Henneman, W., Killiany, R.J., Malykhin, N., Pasqualetti, P., Pruessner, J.C., Redolfi, A., Robitaille, N., Soininen, H., Tolomeo, D., Wang, L., Watson, C., Wolf, H., Duvernoy, H., Duchesne, S., Jack Jr., C.R., Frisoni, G.B., Segmentation, E.-A.W.G. on the H.P. for M.H., 2015a. Delphi definition of the EADC-ADNI Harmonized Protocol for hippocampal segmentation on magnetic resonance. Alzheimers Dement. 11, 126–138. https://doi.org/10.1016/j.jalz.2014.02.009

Boccardi, M., Bocchetta, M., Morency, F.C., Collins, D.L., Nishikawa, M., Ganzola, R., Grothe, M.J., Wolf, D., Redolfi, A., Pievani, M., Antelmi, L., Fellgiebel, A., Matsuda, H., Teipel, S., Duchesne, S., Jack Jr., C.R., Frisoni, G.B., EADC-ADNI Working Group on The Harmonized Protocol for Manual Hippocampal Segmentation and for the Alzheimer's Disease Neuroimaging Initiative, 2015b. Training labels for hippocampal segmentation based on the EADC-ADNI harmonized hippocampal protocol. Alzheimers Dement. 11, 175–183. https://doi.org/10.1016/j.jalz.2014.12.002

Caire, F., Ranoux, D., Guehl, D., Burbaud, P., Cuny, E., 2013. A systematic review of studies on anatomical position of electrode contacts used for chronic subthalamic stimulation in Parkinson's disease. Acta Neurochir. (Wien) 155, 1647–1654. https://doi.org/10.1007/s00701-013-1782-1

Choueib, S., Pinter, C., Lasso, A., Fillion-Robin, J.-C., Vimort, J.-B., Martin, K., Fichtinger, G., 2019. Evaluation of 3D slicer as a medical virtual reality visualization platform, in: Medical Imaging 2019: Image-Guided Procedures, Robotic Interventions, and Modeling. Presented at the Medical Imaging 2019: Image-Guided Procedures, Robotic Interventions, and Modeling, SPIE, pp. 279–286. https://doi.org/10.1117/12.2513053

D'Albis, T., Haegelen, C., Essert, C., Fernández-Vidal, S., Lalys, F., Jannin, P., 2015. PyDBS: an automated image processing workflow for deep brain stimulation surgery. Int. J. Comput. Assist. Radiol. Surg. 10, 117–128. https://doi.org/10.1007/s11548-014-1007-y

Davatzikos, C., Xu, F., An, Y., Fan, Y., Resnick, S.M., 2009. Longitudinal progression of Alzheimer's-like patterns of atrophy in normal older adults: the SPARE-AD index. Brain 132, 2026–2035. https://doi.org/10.1093/brain/awp091

Dembek, T.A., Barbe, M.T., Åström, M., Hoevels, M., Visser-Vandewalle, V., Fink, G.R., Timmermann, L., 2017. Probabilistic mapping of deep brain stimulation effects in essential tremor. NeuroImage Clin. 13, 164–173. https://doi.org/10.1016/j.nicl.2016.11.019

Dembek, T.A., Hellerbach, A., Jergas, H., Eichner, M., Wirths, J., Dafsari, H.S., Barbe, M.T., Hunsche, S., Visser-Vandewalle, V., Treuer, H., 2021. DiODe v2: Unambiguous and Fully-Automated Detection of Directional DBS Lead Orientation. Brain Sci. 11, 1450. https://doi.org/10.3390/brainsci11111450

Dutta, S., Ackermann, E., Kemere, C., 2018. Analysis of an open source, closed-loop, realtime system for hippocampal sharp-wave ripple disruption. J. Neural Eng. 16, 016009. https://doi.org/10.1088/1741-2552/aae90e

Edlow, B.L., Mareyam, A., Horn, A., Polimeni, J.R., Witzel, T., Tisdall, M.D., Augustinack, J.C., Stockmann, J.P., Diamond, B.R., Stevens, A., Tirrell, L.S., Folkerth, R.D., Wald, L.L., Fischl, B., Van Der Kouwe, A., 2019. 7 Tesla MRI of the ex vivo human brain at 100 micron resolution. Sci. Data 6. https://doi.org/10.1038/s41597-019-0254-8

Ewert, S., Horn, A., Finkel, F., Li, N., Kühn, A.A., Herrington, T.M., 2019. Optimization and comparative evaluation of nonlinear deformation algorithms for atlas-based segmentation of DBS target nuclei. NeuroImage 184, 586–598. https://doi.org/10.1016/j.neuroimage.2018.09.061

Ewert, S., Plettig, P., Li, N., Chakravarty, M., Collins, L., Herrington, T., Kühn, A., Horn, A., 2017. Toward defining deep brain stimulation targets in MNI space: A subcortical atlas based on multimodal MRI, histology and structural connectivity. NeuroImage. https://doi.org/10.1016/j.neuroimage.2017.05.015

Fedorov, A., Beichel, R., Kalpathy-Cramer, J., Finet, J., Fillion-Robin, J.-C., Pujol, S., Bauer, C., Jennings, D., Fennessy, F., Sonka, M., Buatti, J., Aylward, S., Miller, J.V., Pieper, S., Kikinis, R., 2012. 3D Slicer as an image computing platform for the Quantitative Imaging Network. Magn. Reson. Imaging 30, 1323–1341. https://doi.org/10.1016/j.mri.2012.05.001

Fonov, V.S., Evans, A.C., McKinstry, R.C., Almli, C.R., Collins, D.L., 2009. Unbiased nonlinear average age-appropriate brain templates from birth to adulthood. NeuroImage 47, S102. https://doi.org/10.1016/S1053-8119(09)70884-5

Forstmann, B.U., Isaacs, B.R., Temel, Y., 2017. Ultra High Field MRI-Guided Deep Brain Stimulation. Trends Biotechnol. 35, 904–907. https://doi.org/10.1016/j.tibtech.2017.06.010

Gadot, R., Vanegas Arroyave, N., Dang, H., Anand, A., Najera, R.A., Taneff, L.Y., Bellows, S., Tarakad, A., Jankovic, J., Horn, A., Shofty, B., Viswanathan, A., Sheth, S.A., 2022. Association of clinical outcomes and connectivity in awake versus asleep deep brain stimulation for Parkinson disease. J. Neurosurg. 1–12. https://doi.org/10.3171/2022.6.JNS212904

Hamani, C., McAndrews, M.P., Cohn, M., Oh, M., Zumsteg, D., Shapiro, C.M., Wennberg, R.A., Lozano, A.M., 2008. Memory enhancement induced by hypothalamic/fornix deep brain stimulation. Ann. Neurol. 63, 119–123. https://doi.org/10.1002/ana.21295

Hariz, M., Lees, A.J., Blomstedt, Y., Blomstedt, P., 2022. Serendipity and Observations in Functional Neurosurgery: From James Parkinson's Stroke to Hamani's & Lozano's Flashbacks. Stereotact. Funct. Neurosurg. 1–9. https://doi.org/10.1159/000525794

Horn, A., 2019. The impact of modern-day neuroimaging on the field of deep brain stimulation. Curr. Opin. Neurol. 32.

Horn, A., Kühn, A.A., 2015. Lead-DBS: A toolbox for deep brain stimulation electrode localizations and visualizations. NeuroImage 107, 127–135. https://doi.org/10.1016/j.neuroimage.2014.12.002

Horn, A., Li, N., Dembek, T.A., Kappel, A., Boulay, C., Ewert, S., Tietze, A., Husch, A., Perera, T., Neumann, W.-J., Reisert, M., Si, H., Oostenveld, R., Rorden, C., Yeh, F.-C., Fang, Q., Herrington, T.M., Vorwerk, J., Kühn, A.A., 2019. Lead-DBS v2: Towards a comprehensive pipeline for deep brain stimulation imaging. NeuroImage 184, 293–316. https://doi.org/10.1016/j.neuroimage.2018.08.068

Horn, A., Reich, M., Vorwerk, J., Li, N., Wenzel, G., Fang, Q., Schmitz-Hübsch, T., Nickl, R., Kupsch, A., Volkmann, J., Kühn, A.A., Fox, M.D., 2017. Connectivity Predicts deep brain stimulation outcome in Parkinson disease. Ann. Neurol. 82, 67–78. https://doi.org/10.1002/ana.24974

Horn, A., Reich, M.M., Ewert, S., Li, N., Al-Fatly, B., Lange, F., Roothans, J., Oxenford, S., Horn, I., Paschen, S., Runge, J., Wodarg, F., Witt, K., Nickl, R.C., Wittstock, M., Schneider, G.-H., Mahlknecht, P., Poewe, W., Eisner, W., Helmers, A.-K.,

Matthies, C., Krauss, J.K., Deuschl, G., Volkmann, J., Kühn, A.A., 2022. Optimal deep brain stimulation sites and networks for cervical vs. generalized dystonia. Proc. Natl. Acad. Sci. 119, e2114985119. https://doi.org/10.1073/pnas.2114985119

Husch, A., V. Petersen, M., Gemmar, P., Goncalves, J., Hertel, F., 2018. PaCER - A fully automated method for electrode trajectory and contact reconstruction in deep brain stimulation. NeuroImage Clin. 17, 80–89. https://doi.org/10.1016/j.nicl.2017.10.004

Iglesias, J.E., Insausti, R., Lerma-Usabiaga, G., Bocchetta, M., Van Leemput, K., Greve, D.N., van der Kouwe, A., Fischl, B., Caballero-Gaudes, C., Paz-Alonso, P.M., 2018. A probabilistic atlas of the human thalamic nuclei combining ex vivo MRI and histology. NeuroImage 183, 314–326. https://doi.org/10.1016/j.neuroimage.2018.08.012

Jenkinson, M., Beckmann, C.F., Behrens, T.E.J., Woolrich, M.W., Smith, S.M., 2012. FSL. NeuroImage, 20 YEARS OF fMRI 62, 782–790. https://doi.org/10.1016/j.neuroimage.2011.09.015

Kapur, T., Pieper, S., Fedorov, A., Fillion-Robin, J.C., Halle, M., O'Donnell, L., Lasso, A., Ungi, T., Pinter, C., Finet, J., Pujol, S., Jagadeesan, J., Tokuda, J., Norton, I., Estepar, R.S.J., Gering, D., Aerts, H.J.W.L., Jakab, M., Hata, N., Ibanez, L., Blezek, D., Miller, J., Aylward, S., Grimson, W.E.L., Fichtinger, G., Wells, W.M., Lorensen, W.E., Schroeder, W., Kikinis, R., 2016. Increasing the impact of medical image computing using community-based open-access hackathons: The NA-MIC and 3D Slicer experience. Med. Image Anal. 33, 176–180. https://doi.org/10.1016/j.media.2016.06.035

Khosravi, M., Atashzar, S.F., Gilmore, G., Jog, M.S., Patel, R.V., 2020. Intraoperative Localization of STN During DBS Surgery Using a Data-Driven Model. IEEE J. Transl. Eng. Health Med. 8, 1–9. https://doi.org/10.1109/JTEHM.2020.2969152

Kikinis, R., Pieper, S.D., Vosburgh, K.G., 2014. 3D Slicer: a platform for subject-specific image analysis, visualization, and clinical support, in: Intraoperative Imaging and Image-Guided Therapy. Springer, pp. 277–289.

Klein, A., Andersson, J., Ardekani, B.A., Ashburner, J., Avants, B., Chiang, M.-C., Christensen, G.E., Collins, D.L., Gee, J., Hellier, P., Song, J.H., Jenkinson, M., Lepage, C., Rueckert, D., Thompson, P., Vercauteren, T., Woods, R.P., Mann, J.J., Parsey, R.V., 2009. Evaluation of 14 nonlinear deformation algorithms applied to human brain MRI registration. NeuroImage 46, 786–802. https://doi.org/10.1016/j.neuroimage.2008.12.037

Koirala, N., Serrano, L., Paschen, S., Falk, D., Anwar, A.R., Kuravi, P., Deuschl, G., Groppa, S., Muthuraman, M., 2020. Mapping of subthalamic nucleus using microelectrode recordings during deep brain stimulation. Sci. Rep. 10. https://doi.org/10.1038/s41598-020-74196-5

Krauss, J.K., Lipsman, N., Aziz, T., Boutet, A., Brown, P., Chang, J.W., Davidson, B., Grill, W.M., Hariz, M.I., Horn, A., Schulder, M., Mammis, A., Tass, P.A., Volkmann, J., Lozano, A.M., 2021. Technology of deep brain stimulation: current status and future directions. Nat. Rev. Neurol. 17, 75–87. https://doi.org/10.1038/s41582-020-00426-z

Krüger, M., Várkuti, B., Achinger, J., Volker, Prokop, T., Delev, D., Blass, B.-I., Piroth, T., Peter, 2020. Navigated Deep Brain Stimulation Surgery: Evaluating the Combined Use of a Frame-Based Stereotactic System and a Navigation System. Stereotact. Funct. Neurosurg. 1–7. https://doi.org/10.1159/000510528

Kuncel, A.M., Cooper, S.E., Grill, W.M., 2008. A method to estimate the spatial extent of activation in thalamic deep brain stimulation. Clin. Neurophysiol. 119, 2148–2158. https://doi.org/10.1016/j.clinph.2008.02.025

Lee, A.T., Han, K.J., Nichols, N., Sudhakar, V.R., Burke, J.F., Wozny, T.A., Chung, J.E., Volz, M.M., Ostrem, J.L., Martin, A.J., Larson, P.S., Starr, P.A., Wang, D.D., 2022. Targeting Accuracy and Clinical Outcomes of Awake versus Asleep Interventional Magnetic Resonance Imaging-Guided Deep Brain Stimulation for Parkinson's Disease: The University of California, San Francisco Experience. Neurosurgery 91, 717–725. https://doi.org/10.1227/neu.0000000000002111

Li, N., Baldermann, J.C., Kibleur, A., Treu, S., Akram, H., Elias, G.J.B., Boutet, A., Lozano, A.M., Al-Fatly, B., Strange, B., Barcia, J.A., Zrinzo, L., Joyce, E., Chabardes, S., Visser-Vandewalle, V., Polosan, M., Kuhn, J., Kühn, A.A., Horn, A., 2020. A unified connectomic target for deep brain stimulation in obsessive-compulsive disorder. Nat. Commun. 11. https://doi.org/10.1038/s41467-020-16734-3

Lozano, A.M., Lipsman, N., Bergman, H., Brown, P., Chabardes, S., Chang, J.W., Matthews, K., McIntyre, C.C., Schlaepfer, T.E., Schulder, M., Temel, Y., Volkmann, J., Krauss, J.K., 2019. Deep brain stimulation: current challenges and future directions. Nat. Rev. Neurol. 15, 148–160. https://doi.org/10.1038/s41582-018-0128-2

Lozano, C.S., Ranjan, M., Boutet, A., Xu, D.S., Kucharczyk, W., Fasano, A., Lozano, A.M., 2019. Imaging alone versus microelectrode recording–guided targeting of the STN in patients with Parkinson's disease. J. Neurosurg. 130, 1847–1852. https://doi.org/10.3171/2018.2.jns172186

Mädler, B., Coenen, V.A., 2012. Explaining Clinical Effects of Deep Brain Stimulation through Simplified Target-Specific Modeling of the Volume of Activated Tissue. Am. J. Neuroradiol. 33, 1072–1080. https://doi.org/10.3174/ajnr.A2906

Martin, A.J., Larson, P.S., Ostrem, J.L., Keith Sootsman, W., Talke, P., Weber, O.M., Levesque, N., Myers, J., Starr, P.A., 2005. Placement of deep brain stimulator electrodes using real-time high-field interventional magnetic resonance imaging. Magn. Reson. Med. 54, 1107–1114. https://doi.org/10.1002/mrm.20675

McIntyre, C.C., Grill, W.M., Sherman, D.L., Thakor, N.V., 2004. Cellular Effects of Deep Brain Stimulation: Model-Based Analysis of Activation and Inhibition. J. Neurophysiol. 91, 1457–1469. https://doi.org/10.1152/jn.00989.2003

Miller, W.C., DeLong, M.R., 1988. Parkinsonian Symptomatology An Anatomical and Physiological Analysisaa. Ann. N. Y. Acad. Sci. 515, 287–302. https://doi.org/10.1111/j.1749-6632.1988.tb32998.x

Neudorfer, C., Butenko, K., Oxenford, S., Rajamani, N., Achtzehn, J., Goede, L., Hollunder, B., Ríos, A.S., Hart, L., Tasserie, J., Fernando, K.B., Nguyen, T.A.K., Al-Fatly, B., Vissani, M., Fox, M., Richardson, R.M., van Rienen, U., Kühn, A.A., Husch, A.D., Opri, E., Dembek, T., Li, N., Horn, A., 2023. Lead-DBS v3.0: Mapping

Deep Brain Stimulation Effects to Local Anatomy and Global Networks. NeuroImage 119862. https://doi.org/10.1016/j.neuroimage.2023.119862

Noecker, A.M., Frankemolle-Gilbert, A.M., Howell, B., Petersen, M.V., Beylergil, S.B., Shaikh, A.G., McIntyre, C.C., 2021. StimVision v2: Examples and Applications in Subthalamic Deep Brain Stimulation for Parkinson's Disease. Neuromodulation Technol. Neural Interface 24, 248–258. https://doi.org/10.1111/ner.13350

Noecker, A.M., Mlakar, J., Petersen, M.V., Griswold, M.A., McIntyre, C.C., 2023. Holographic visualization for stereotactic neurosurgery research. Brain Stimulat. 16, 411–414. https://doi.org/10.1016/j.brs.2023.02.001

Oxenford, S., Roediger, J., Neudorfer, C., Milosevic, L., Güttler, C., Spindler, P., Vajkoczy, P., Neumann, W.-J., Kühn, A., Horn, A., 2022. Lead-OR: A multimodal platform for deep brain stimulation surgery. eLife 11, e72929. https://doi.org/10.7554/eLife.72929

Petersen, M.V., Mlakar, J., Haber, S.N., Parent, M., Smith, Y., Strick, P.L., Griswold, M.A., McIntyre, C.C., 2019. Holographic Reconstruction of Axonal Pathways in the Human Brain. Neuron 104, 1056-1064 e3. https://doi.org/10.1016/j.neuron.2019.09.030

Ríos, A.S., Oxenford, S., Neudorfer, C., Butenko, K., Li, N., Rajamani, N., Boutet, A., Elias, G.J.B., Germann, J., Loh, A., Deeb, W., Wang, F., Setsompop, K., Salvato, B., Almeida, L.B. de, Foote, K.D., Amaral, R., Rosenberg, P.B., Tang-Wai, D.F., Wolk, D.A., Burke, A.D., Salloway, S., Sabbagh, M.N., Chakravarty, M.M., Smith, G.S., Lyketsos, C.G., Okun, M.S., Anderson, W.S., Mari, Z., Ponce, F.A., Lozano, A.M., Horn, A., 2022. Optimal deep brain stimulation sites and networks for stimulation of the fornix in Alzheimer's disease. Nat. Commun. 13, 7707. https://doi.org/10.1038/s41467-022-34510-3

Schulder, M., Mishra, A., Mammis, A., Horn, A., Boutet, A., Blomstedt, P., Chabardes, S., Flouty, O., Lozano, A.M., Neimat, J.S., Ponce, F., Starr, P.A., Krauss, J.K., Hariz, M., Chang, J.W., 2023. Advances in Technical Aspects of Deep Brain Stimulation Surgery. Stereotact. Funct. Neurosurg. 1–23. https://doi.org/10.1159/000529040

Siegle, J.H., López, A.C., Patel, Y.A., Abramov, K., Ohayon, S., Voigts, J., 2017. Open Ephys: an open-source, plugin-based platform for multichannel electrophysiology. J. Neural Eng. 14, 045003. https://doi.org/10.1088/1741-2552/aa5eea

Sobesky, L., Goede, L., Odekerken, V.J.J., Wang, Q., Li, N., Neudorfer, C., Rajamani, N., Al-Fatly, B., Reich, M., Volkmann, J., de Bie, R.M.A., Kühn, A.A., Horn, A., 2022. Subthalamic and pallidal deep brain stimulation: are we modulating the same network? Brain 145, 251–262. https://doi.org/10.1093/brain/awab258

Starr, P.A., Christine, C.W., Theodosopoulos, P.V., Lindsey, N., Byrd, D., Mosley, A., Marks, W.J., 2002. Implantation of deep brain stimulators into subthalmic nucleus: technical approach and magnetic imaging—verified electrode locations. J. Neurosurg. 97, 370–387.

Tao, S., Zhou, X., Lin, C., Patel, V., Westerhold, E.M., Middlebrooks, E.H., 2023. Optimization of MP2RAGE T1 mapping with radial view-ordering for deep brain stimulation targeting at 7 T MRI. Magn. Reson. Imaging. https://doi.org/10.1016/j.mri.2023.03.007

Thompson, J.A., Oukal, S., Bergman, H., Ojemann, S., Hebb, A.O., Hanrahan, S., Israel, Z., Abosch, A., 2018. Semi-automated application for estimating subthalamic nucleus boundaries and optimal target selection for deep brain stimulation implantation surgery. J. Neurosurg. 1–10. https://doi.org/10.3171/2017.12.jns171964

Tokuda, J., Fischer, G.S., Papademetris, X., Yaniv, Z., Ibanez, L., Cheng, P., Liu, H., Blevins, J., Arata, J., Golby, A.J., Kapur, T., Pieper, S., Burdette, E.C., Fichtinger, G., Tempany, C.M., Hata, N., 2009. OpenIGTLink: an open network protocol for image-guided therapy environment. Int. J. Med. Robot. 5, 423–434. https://doi.org/10.1002/rcs.274

Treu, S., Strange, B., Oxenford, S., Neumann, W.-J., Kühn, A., Li, N., Horn, A., 2020. Deep brain stimulation: Imaging on a group level. NeuroImage 219, 117018. https://doi.org/10.1016/j.neuroimage.2020.117018

Ungi, T., Lasso, A., Fichtinger, G., 2016. Open-source platforms for navigated image-guided interventions. Med. Image Anal. 33, 181–186. https://doi.org/10.1016/j.media.2016.06.011

Valsky, D., Blackwell, K.T., Tamir, I., Eitan, R., Bergman, H., Israel, Z., 2020. Real-time machine learning classification of pallidal borders during deep brain stimulation surgery. J. Neural Eng. 17, 016021. https://doi.org/10.1088/1741-2552/ab53ac

Valsky, D., Marmor-Levin, O., Deffains, M., Eitan, R., Blackwell, K.T., Bergman, H., Israel, Z., 2017. Stop! border ahead: Automatic detection of subthalamic exit during deep brain stimulation surgery. Mov. Disord. 32, 70–79. https://doi.org/10.1002/mds.26806

Vinke, R.S., Geerlings, M., Selvaraj, A.K., Georgiev, D., Bloem, B.R., Esselink, R.A.J., Bartels, R.H.M.A., 2022. The Role of Microelectrode Recording in Deep Brain Stimulation Surgery for Parkinson's Disease: A Systematic Review and Meta-Analysis. J. Park. Dis. Preprint, 1–11. https://doi.org/10.3233/JPD-223333

Wolf, D., Bocchetta, M., Preboske, G.M., Boccardi, M., Grothe, M.J., 2017. Reference standard space hippocampus labels according to the European Alzheimer's Disease Consortium–Alzheimer's Disease Neuroimaging Initiative harmonized protocol: Utility in automated volumetry. Alzheimers Dement. 13, 893–902. https://doi.org/10.1016/j.jalz.2017.01.009

Zaidel, A., Spivak, A., Grieb, B., Bergman, H., Israel, Z., 2010. Subthalamic span of oscillations predicts deep brain stimulation efficacy for patients with Parkinson's disease. Brain 133, 2007–2021. https://doi.org/10.1093/brain/awq144

Zaidel, A., Spivak, A., Shpigelman, L., Bergman, H., Israel, Z., 2009. Delimiting subterritories of the human subthalamic nucleus by means of microelectrode recordings and a Hidden Markov Model. Mov. Disord. 24, 1785–1793. https://doi.org/10.1002/mds.22674

Zrinzo, L., Foltynie, T., Limousin, P., Hariz, M.I., 2012. Reducing hemorrhagic complications in functional neurosurgery: a large case series and systematic literature review: Clinical article. J. Neurosurg. JNS 116, 84–94. https://doi.org/10.3171/2011.8.Jns101407

Statutory Declaration

“I, Simon Oxenford, by personally signing this document in lieu of an oath, hereby affirm that I prepared the submitted dissertation on the topic *Multimodal navigation in deep brain stimulation surgery (Multimodale Navigation in der Tiefenhirnstimulationschirurgie)*, independently and without the support of third parties, and that I used no other sources and aids than those stated.

All parts which are based on the publications or presentations of other authors, either in letter or in spirit, are specified as such in accordance with the citing guidelines. The sections on methodology (in particular regarding practical work, laboratory regulations, statistical processing) and results (in particular regarding figures, charts and tables) are exclusively my responsibility.

Furthermore, I declare that I have correctly marked all of the data, the analyses, and the conclusions generated from data obtained in collaboration with other persons, and that I have correctly marked my own contribution and the contributions of other persons (cf. declaration of contribution). I have correctly marked all texts or parts of texts that were generated in collaboration with other persons.

My contributions to any publications to this dissertation correspond to those stated in the below joint declaration made together with the supervisor. All publications created within the scope of the dissertation comply with the guidelines of the ICMJE (International Committee of Medical Journal Editors; http://www.icmje.org) on authorship. In addition, I declare that I shall comply with the regulations of Charité – Universitätsmedizin Berlin on ensuring good scientific practice.

I declare that I have not yet submitted this dissertation in identical or similar form to another Faculty.

The significance of this statutory declaration and the consequences of a false statutory declaration under criminal law (Sections 156, 161 of the German Criminal Code) are known to me.”

Date Signature

Declaration of your own contribution to the publications

Simon Oxenford contributed the following to the below listed publications:

Publication 1: Simón Oxenford, Jan Roediger, Clemens Neudorfer, Luka Milosevic, Christopher Güttler, Philipp Spindler, Peter Vajkoczy, Wolf-Julian Neumann, Andrea Kühn, Andreas Horn, *Lead-OR: A multimodal platform for deep brain stimulation surgery*, eLife, 2022

Contribution: I conceptualized this study together with my supervisor Andreas Horn; I gathered the data with help from Philipp Spindler and Jan Roediger; I performed all the investigation and analysis under guidance of my supervisor Andreas horn; I developed the software platform Lead-OR described in the publication (authored 97% of commits; see detailed code contribution here: https://github.com/netstim/SlicerNetstim/graphs/contributors); I am one of the developers of Lead-DBS toolbox also used in some analysis in the publication (see detailed code contribution here: https://github.com/netstim/leaddbs/graphs/contributors); I created all the figures of the publication. I wrote the first draft of the manuscript and reviewed the written contribution from co-authors.

_____

Signature, date and stamp of first supervising university professor / lecturer

_____

Signature of doctoral candidate

Excerpt from Journal Summary List

Journal Data Filtered By: **Selected JCR Year: 2021** Selected Editions: SCIE,SSCI
Selected Categories: **"BIOLOGY"** Selected Category Scheme: WoS
Gesamtanzahl: 94 Journale

Rank	Full Journal Title	Total Cites	Journal Impact Factor	Eigenfaktor
1	BIOLOGICAL REVIEWS	19,206	14.350	0.01915
2	BIOSCIENCE	24,496	11.566	0.01178
3	CURRENT BIOLOGY	85,124	10.900	0.10641
4	Science China-Life Sciences	7,316	10.372	0.01077
5	Physics of Life Reviews	2,121	9.833	0.00290
6	PLOS BIOLOGY	44,888	9.593	0.05920
7	BioScience Trends	2,711	9.083	0.00339
8	eLife	89,502	8.713	0.28523
9	BIOLOGICAL RESEARCH	3,299	7.634	0.00235
10	BMC BIOLOGY	10,352	7.364	0.01595
11	Biology Direct	2,618	7.173	0.00175
12	QUARTERLY REVIEW OF BIOLOGY	4,824	6.750	0.00081
13	COMPUTERS IN BIOLOGY AND MEDICINE	14,531	6.698	0.01430
14	PHILOSOPHICAL TRANSACTIONS OF THE ROYAL SOCIETY B-BIOLOGICAL SCIENCES	62,963	6.671	0.05133
15	Communications Biology	11,444	6.548	0.02842
16	FASEB JOURNAL	59,831	5.834	0.04452
17	Life Science Alliance	2,253	5.781	0.00643
18	BIOELECTROCHEMISTRY	7,093	5.760	0.00463
19	PROCEEDINGS OF THE ROYAL SOCIETY B-BIOLOGICAL SCIENCES	67,725	5.530	0.05142
20	Current Opinion in Insect Science	4,250	5.254	0.00722
21	Biology-Basel	6,091	5.168	0.00693
22	Interface Focus	3,459	4.661	0.00471
23	BIOESSAYS	12,321	4.653	0.01097
24	Geobiology	2,977	4.216	0.00329
25	SAUDI JOURNAL OF BIOLOGICAL SCIENCES	9,217	4.052	0.00759
26	ASTROBIOLOGY	5,156	4.045	0.00581
27	EXCLI Journal	3,177	4.022	0.00276
28	MATHEMATICAL BIOSCIENCES	8,137	3.935	0.00445
29	BULLETIN OF MATHEMATICAL BIOLOGY	6,593	3.871	0.00637
30	Biology Letters	13,630	3.812	0.01319
31	CHRONOBIOLOGY INTERNATIONAL	8,768	3.749	0.00621

Printing copy(s) of the publication(s)

eLife

TOOLS AND RESOURCES

Lead-OR: A multimodal platform for deep brain stimulation surgery

Simón Oxenford[1*†], Jan Roediger[1,2], Clemens Neudorfer[1,3,4], Luka Milosevic[5,6], Christopher Güttler[1], Philipp Spindler[7], Peter Vajkoczy[7], Wolf-Julian Neumann[1], Andrea Kühn[1], Andreas Horn[1,3,4]

[1]Movement Disorders and Neuromodulation Unit, Department of Neurology, Charité — Universitätsmedizin Berlin, corporate member of Freie Universität Berlin and Humboldt Universität zu Berlin, Berlin, Germany; [2]Charité — Universitätsmedizin Berlin, Einstein Center for Neurosciences Berlin, Berlin, Germany; [3]Center for Brain Circuit Therapeutics Department of Neurology, Brigham & Women's Hospital, Harvard Medical School, Boston, United States; [4]MGH Neurosurgery & Center for Neurotechnology and Neurorecovery (CNTR) at MGH Neurology Massachusetts General Hospital, Harvard Medical School, Boston, United States; [5]Institute of Biomedical Engineering, University of Toronto, Toronto, Canada; [6]Krembil Brain Institute, University Health Network, Toronto, Canada; [7]Department of Neurosurgery, Charité — Universitätsmedizin Berlin, Berlin, Germany

***For correspondence:** simon.oxenford@charite.de

Present address: †Movement Disorders and Neuromodulation Unit, Department for Neurology, Charité — Universitätsmedizin, Berlin, Germany

Competing interest: See page 16

Funding: See page 16

Received: 09 August 2021
Preprinted: 10 August 2021
Accepted: 19 May 2022
Published: 20 May 2022

Reviewing Editor: Lars Timmermann, University Hospital of Gießen and Marburg, Germany

Abstract

Background: Deep brain stimulation (DBS) electrode implant trajectories are stereotactically defined using preoperative neuroimaging. To validate the correct trajectory, microelectrode recordings (MERs) or local field potential recordings can be used to extend neuroanatomical information (defined by MRI) with neurophysiological activity patterns recorded from micro- and macroelectrodes probing the surgical target site. Currently, these two sources of information (imaging vs. electrophysiology) are analyzed separately, while means to fuse both data streams have not been introduced.

Methods: Here, we present a tool that integrates resources from stereotactic planning, neuroimaging, MER, and high-resolution atlas data to create a real-time visualization of the implant trajectory. We validate the tool based on a retrospective cohort of DBS patients (N = 52) offline and present single-use cases of the real-time platform.

Results: We establish an open-source software tool for multimodal data visualization and analysis during DBS surgery. We show a general correspondence between features derived from neuroimaging and electrophysiological recordings and present examples that demonstrate the functionality of the tool.

Conclusions: This novel software platform for multimodal data visualization and analysis bears translational potential to improve accuracy of DBS surgery. The toolbox is made openly available and is extendable to integrate with additional software packages.

Funding: Deutsche Forschungsgesellschaft (410169619, 424778381), Deutsches Zentrum für Luft- und Raumfahrt (DynaSti), National Institutes of Health (2R01 MH113929), and Foundation for OCD Research (FFOR).

Editor's evaluation

The authors present a software tool combining and correlating the documentation of intraoperative neurophysiological findings with atlas and imaging data. They also show an exemplary validation

of their tool in a clinical series of 52 Parkinson's disease patients who underwent DBS surgery. This article will be of interest to clinicians and researchers who are involved in both the placement and controlling of the accuracy of the location of deep brain stimulation electrodes.

Introduction

During deep brain stimulation (DBS) surgery, different sources of information are used to ensure precise placement of the electrodes within the target structure. Functional stereotactic coordinates (defined relative to anatomical atlas landmarks) are often used as a starting point (indirect targeting). Then, more importantly, preoperative MRI sequences optimized to visualize target structures are used to refine the initial plan (direct targeting). Surgical planning is usually carried out after fusing the MRI sequences with a computed tomography (CT) volume acquired with the stereotactic frame and fiducial plates already mounted to the patient's head. The fiducial plates include markers that are used to convert stereotactic coordinates (established in the planning software) to frame coordinates (applicable to mechanically adjust the stereotactic frame) in order to place electrodes to the intended target.

During the surgical procedure, microelectrode recordings (MERs), as well as test stimulations carried out using macroelectrodes, are often used as an additional confirmation step of placement in the intended target site. While the necessity of the former step has been debated (***Aviles-Olmos et al., 2014***) and the procedure may lead to slightly increased rates of complications (***Zrinzo et al., 2012***), the experience of our own high-volume center is that roughly every fifth patient's surgical plan will be slightly altered based on electrophysiological signals, with similar experiences reported by others (***Lozano et al., 2018***). Of specific relevance is the role of brain shift occurring due to air entering the skull during surgery: even with optimal imaging and meticulous surgical planning beforehand, brain shift may lead to nonlinear displacement of the brain relative to the skull and stereotactic frame (***Halpern et al., 2008***), which can only be monitored intraoperatively (e.g., using the electrophysiological data recorded with microelectrode probes). While most centers analyze MERs by visual and auditory inspection from expert neurosurgeons or neurologists, the first FDA and CE-approved machine-learning algorithms that facilitate this monitoring step have recently been introduced, for instance, in the form of the HaGuide system created by the company Alpha Omega Engineering (Nazareth, Israel; ***Thompson et al., 2018***).

Still, understanding and communicating the complex neuroanatomical and neurophysiological relationships within the clinical team during the procedure may remain a challenge even for experts. To account for this, ***Krüger, 2020*** introduced the concept of navigated DBS surgery, showing that a visual feedback of the microelectrode position can be helpful to mentally envision the ongoing 3D scene.

In parallel, reconstructions of DBS target regions based on elaborate MRI sequences have become increasingly precise (***Horn, 2019***; ***Krauss et al., 2021***). Specialized MRI sequences have been introduced to maximize visibility and boundary definitions of pallidal, thalamic (***Tourdias et al., 2014***; ***Sudhyadhom et al., 2009***; ***Vassal et al., 2012***), and subthalamic (***Santin et al., 2017***; ***Wang and Liu, 2015***) targets. But even when relying on a set of standard sequences (e.g., T1 and T2), modern reconstruction pipelines have the capability to reconstruct the subthalamic nucleus (STN) and internal segment of the globus pallidus (GPi) with a precision that rivals manual expert segmentations (***Ewert et al., 2019***). Over recent years, these methods have made it possible to transform the 2D representations of stereotactic imaging slices into 3D models that are not only graphically appealing but indeed realistic and meaningful (***Horn and Kühn, 2015***). As a by-product, these tools have made it possible to accurately register atlas data into the patient-specific model. With *atlas data*, here, we generally refer to an array of ultra-high-resolution imaging resources that could be based on histology (***Ilinsky et al., 2018***; ***Ewert et al., 2018***; ***Amunts et al., 2013***), postmortem MRI (***Edlow et al., 2019***), or even expert anatomical knowledge aggregated in three-dimensional fashion (***Petersen et al., 2019***). Similarly, atlas data could represent optimal stimulation sites defined on a group level, for instance, in the form of probabilistic sweet spot targets (***Dembek et al., 2019***; ***Boutet et al., 2021***; ***Elias et al., 2021***; ***Horn et al., 2017***) or tractography-defined DBS target atlases (***Li et al., 2020***; ***Treu et al., 2020***; ***Al-Fatly et al., 2019***).

eLife digest Deep brain stimulation is an established therapy for patients with Parkinson's disease and an emerging option for other neurological conditions. Electrodes are implanted deep in the brain to stimulate precise brain regions and control abnormal brain activity in those areas. The most common target for Parkinson's disease, for instance, is a structure called the subthalamic nucleus, which sits at the base of the brain, just above the brain stem.

To ensure electrodes are placed correctly, surgeons use various sources of information to characterize the patient's brain anatomy and decide on an implant site. These data include brain scans taken before surgery and recordings of brain activity taken during surgery to confirm the intended implant site. Sometimes, the brain activity signals from this last confirmation step may slightly alter surgical plans. It represents one of many challenges for clinical teams: to analyse, assimilate, and communicate data as it is collected during the procedure.

Oxenford et al. developed a software pipeline to aggregate the data surgeons use to implant electrodes. The open-source platform, dubbed Lead-OR, visualises imaging data and brain activity recordings (termed electrophysiology data) in real time. The current set-up integrates with commercial tools and existing software for surgical planning.

Oxenford et al. tested Lead-OR on data gathered retrospectively from 32 patients with Parkinson's who had electrodes implanted in their subthalamic nucleus. The platform showed good agreement between imaging and electrophysiology data, although there were some unavoidable discrepancies, arising from limitations in the imaging pipeline and from the surgical procedure. Lead-OR was also able to correct for brain shift, which is where the brain moves ever so slightly in the skull.

With further validation, this proof-of-concept software could serve as a useful decision-making tool for surgical teams implanting electrodes for deep brain stimulation. In time, if implemented, its use could improve the accuracy of electrode placement, translating into better surgical outcomes for patients. It also has the potential to integrate forthcoming ultra-high-resolution data from current brain mapping projects, and other commercial surgical planning tools.

Here, we present an integrative approach to combine information derived from neuroimaging and neurophysiology in a joint visualization platform. First, we build on recent validations of subcortical normalization routines to introduce a method to refine 3D models of subcortical targets on a single patient level. Second, we port our methodology for postoperative electrode localization established within Lead-DBS software (https://www.lead-dbs.org; ***Horn and Kühn, 2015***) to the pre- and intraoperative realm, that is, the one of stereotactic planning, MERs, and intraoperative testing. To achieve this, we present and validate a novel unified software framework termed Lead-OR that incorporates the following resources into a live visualization scene: (1) patient-specific imaging, (2) stereotactic planning information, (3) real-time microelectrode localization, (4) MER feature extraction, and (5) high-resolution atlas imaging data. The capability of the system to integrate electrophysiological information with imaging data is explored in-depth. Beyond this feature, the tool also includes the possibility to visualize test stimulations and real-time fiber tractography. The software framework is made available as an open-source package (https://github.com/netstim/SlicerNetstim) and currently supports integration with the Brainlab Elements (Brainlab AG, Munich, Germany) planning software and a direct interface to the NeuroOmega system (Alpha Omega Engineering). Further integrations with other systems are planned in the future.

Methods

Ethics statement

Lead-OR is intended for purely academic research use and does not have any form of government body regulatory approval. As such, any use of Lead-OR is strictly limited to Institutional Review Board (IRB)-approved research studies at individual academic institutions, while legal frameworks and practices may differ from country to country. The collection and analysis of all patient data used for this article were approved by the local ethics committee of Charité – Universitätsmedizin Berlin (master vote EA2/145/21). All data were analyzed retrospectively and obtained in deidentified form

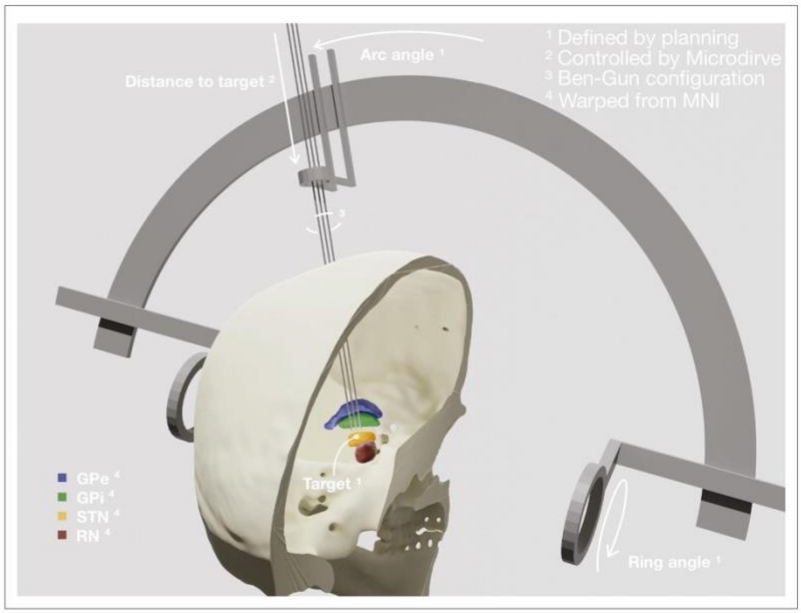

Figure 1. Patient-specific visualization generated by aggregating different sources of data. The stereotactic planning procedure defines the surgical target coordinate, as well as ring and arc angles, which together describe the central trajectory. The Ben-Gun configuration presented in the figure shows additional posterolateral and anteromedial trajectories, 2 mm apart from the central one. Up to five trajectories are currently supported by the software. In our current setup, the distance to the target is controlled by the NeuroOmega system, accessed with its Software Development Kit (SDK) – but can alternatively be set manually within the tool itself. Relevant subcortical nuclei have been warped to patient space via a manually refined normalization. GPe: external segment of the globus pallidus; GPi: internal segment of the globus pallidus; STN: subthalamic nucleus; RN: red nucleus.

from Medical Records of Charité. Hence, following local guidelines in Berlin/Brandenburg as well as NIH guidelines for human subjects research, no explicit patient consent to analyze and publish was obtained/necessary.

Implementation environment

The tools used in this study are implemented in the form of a 3D Slicer (Slicer) (***Fedorov et al., 2012***; ***Kapur et al., 2016***) extension (https://github.com/netstim/SlicerNetstim). The main module of the SlicerNetstim extension is Lead-OR, which assembles the different sources of information, as outlined in the following sections.

Coordinate systems

The first step in aggregating data from different sources is to co-register their spatial relationship and coordinate systems (***Figure 1***). Lead-OR is based on Slicer's world-coordinate system (RAS). We use a linear transform to match the Head-Ring center and positive axes to the origin of this world-coordinate system. The planned central trajectory is then defined based on target coordinates, mounting type, and ring and arc angles. The other trajectories are defined relative to the central one, following the configuration of the Ben-Gun microarray. As mentioned, currently, support for the NeuroOmega setup has been implemented, which uses a Ben-Gun array first introduced by the team of Alim-Louis Benabid (***Benazzouz et al., 2002***).

These trajectories describe a line in space through which the macro, micro, and definitive DBS electrodes are inserted. The last parameter to fully define their position varies throughout surgery,

namely, the distance to the planned target. This parameter is set by the Microdrive, which allows to move the electrodes along the trajectories while recording from the tip of the microelectrodes. In our current setup, this value is queried via the NeuroOmega Software Development Kit (SDK) and alternatively can be manually controlled within the software itself. Interfacing to similar systems as the NeuroOmega device will be possible given the open-source nature of our tool and creating such interfaces with other systems is in our interest for the future.

To co-register the patient's images and frame reference, the tool uses a set of fiducial points defined in both coordinate systems (image and frame) that we extract from the surgical planning coordinates. Specifically, the anterior commissure (AC) and posterior commissure (PC), as well as a midsagittal point (MS), are used to create the transform (implemented using the fiducial registration module available within Slicer). Currently, an interface with the Brainlab Elements (Brainlab AG) stereotactic planning software is implemented (via PDF export in Elements and automated import in Lead-OR). Again, support for alternative planning tools is planned for the future.

Finally, we incorporate high-resolution atlas resources into the patient-specific visualization scene. For the present examples within the article, we used nuclei from the DISTAL (***Ewert et al., 2018***) and MNI PD 25 histology atlases (***Xiao et al., 2017***) that were defined in MNI space (ICBM 2009b Nonlinear Asymmetric, ***Fonov et al., 2009***). Similarly, we imported histological sections from the BigBrain atlas (***Amunts et al., 2013***) and fiber tract definitions provided by the holographic basal ganglia pathway atlas (***Petersen et al., 2019***). In the same fashion, virtually any type of atlas data could be imported to the patient scene, but it is crucial that this registration is of utmost precision. To account for this, we built on the long-standing methods development within Lead-DBS (***Horn and Kühn, 2015***; ***Horn et al., 2019***; ***Ewert et al., 2019***; ***Vogel et al., 2020***; ***Edlow et al., 2019***) but drastically extended the procedure with a novel manual refinement method, termed WarpDrive. Namely, an initial deformation field was calculated via a multispectral four-stage normalization step using the symmetric normalization (SyN) transformation model implemented within Advanced Normalization Tools (ANTs; http://stnava.github.io/ANTs/; ***Avants et al., 2008***). This was implemented using the 'effective: low variance + subcortical refinement' preset defined in Lead-DBS, which has been optimized for normalization of subcortical structures (***Horn et al., 2019***) and has shown to yield accurate

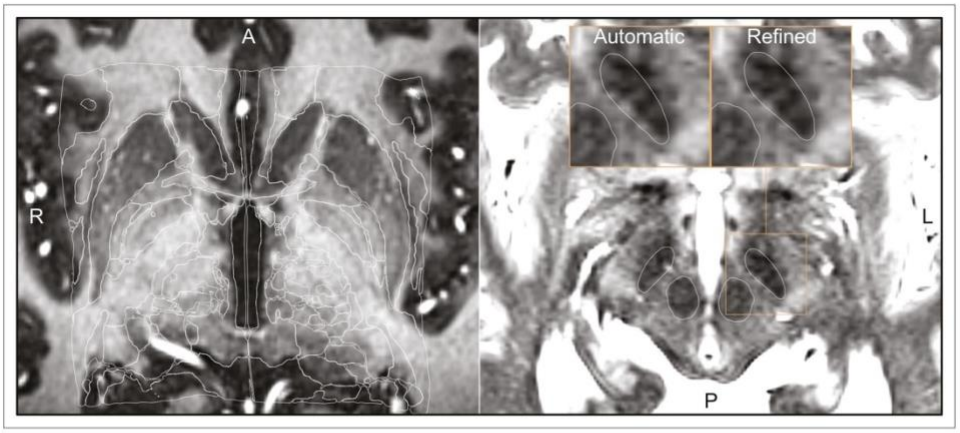

Figure 2. Output of a Lead-DBS/Advanced Normalization Tools (ANTs)-based automated normalization with and without subsequent manual refinement. Two MRI modalities are shown anterior commissure-posterior commissure (AC-PC) aligned: T1-MPRAGE (left) and T2-TSE (right). Both MRI modalities (together with FGATIR, not shown here) were used as an input to the normalization step implemented in Lead-DBS, which allows multispectral registration using ANTs. The white outline shows atlases: MNI PD 25 histology (***Xiao et al., 2017***) (left) and DISTAL (***Ewert et al., 2018***) (right), both included within Lead-DBS.

The online version of this article includes the following video for figure 2:

Figure 2—video 1. General overview of the visualizations and tools made available through the WarpDrive module implementation in Slicer.
https://elifesciences.org/articles/72929/figures#fig2video1

segmentations of subcortical nuclei that rival the ones carried out manually by experts (***Ewert et al., 2019***; ***Vogel et al., 2020***). The deformation fields derived from this automated step are then further manually refined using WarpDrive, which is described in the next section.

Normalization refinement

While normalization algorithms have become increasingly accurate (***Vogel et al., 2020***; ***Ewert et al., 2019***), their precision is not always perfect in single subjects and shows varying accuracy throughout the brain. Indeed, accurate automated registration of the basal ganglia nuclei presents a challenge to intensity-based registration methods given their low contrast between regions (***Ewert et al., 2019***).

Using WarpDrive, an experienced user can recognize such mismatches included in the automated normalization and manually refine the displacement field using point-to-point and line-to-line fiducials as well as a smudge tool. Manually entered fiducials are fed into the Plastimatch software (***Sharp et al., 2010***) (accessed as a command line module from within Slicer). Details about the WarpDrive tool will be reported and evaluated elsewhere. ***Figure 2*** shows an example of a manually refined normalization, and ***Figure 2—video 1*** shows a demo application of the tool to refine atlas-to-patient fits in a surgical case.

Real-time implementation

Lead-OR has the potential to be used in real-time during surgery. As mentioned above, one aspect of this is the continuous/live updating of the microelectrode distance to the surgical target while keeping the scene (i.e., multiple 2D and 3D views) synchronized. The interface to the NeuroOmega device

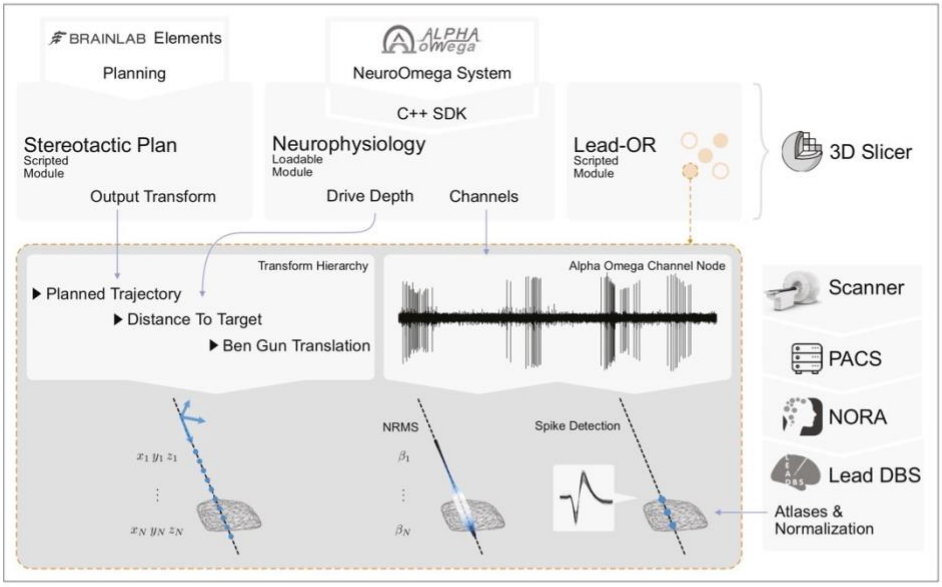

Figure 3. Overview of the SlicerNetstim extension. The current setup shows interfaces with specific commercial products. Similar interfaces to competing tools are planned and will be included in the future. A PDF plan exported from Brainlab Elements is used as an input to the Stereotactic Plan module to store the planned trajectory as a Slicer Transform. The NeuroOmega system is connected via its Software Development Kit (SDK) through the Neurophysiology module, providing continuous updates about the drive depth and electrophysiological channel input. Finally, in the Lead-OR module, the Ben-Gun configuration is defined by selecting the used trajectories and assigning them to input channels from the NeuroOmega device. Using a transform hierarchy, the spatial position of the microelectrode is defined: the Ben-Gun translation is transformed by the distance to the target, this one itself being transformed by the planned trajectory. By doing so, the features extracted from the respective microelectrode recordings (MERs) can be mapped to their spatial location. At our center, an automatic pipeline for preprocessing data retrieved from a picture archiving and communication system (PACS) system is setup using the NORA medical imaging platform (https://www.nora-imaging.com/) to automatically run the core Lead-DBS pipeline once images arrive in the hospital's PACS system. This part (right-hand side) is not discussed in detail since it is largely specific to our center.

provides live data about how distant the microelectrodes are to the target and also streams out electrophysiological recordings made in a real-time manner. Finally, test stimulations can be visualized, including a function for live-tractography visualization estimating 'activated' or 'modulated' tracts.

To make this possible, we included the NeuroOmega C++ SDK as part of a Slicer loadable module. This module sets up the connection to the NeuroOmega device and queries the distance to the target in specified time intervals. It also displays the available channels from which recorded electrophysiological data can be streamed, stored, processed, and visualized.

Through the Lead-OR module, the microelectrode Ben-Gun configuration is defined and the NeuroOmega channels are linked to the selected trajectories. Together with the aforementioned image-to-frame transform, as well as the distance to the target, this allows to define the anatomical location of the electrophysiological signal in real time. The features extracted from recordings are projected into the patient-specific space and represented in the 2D/3D visualization (***Figure 3***). The computation of features is continuously executed for each position of the microdrive, updating the recording stream at each time point. This process takes a few seconds (depending on available hardware), and the visualization is then updated.

(Re-)developing a signal processing pipeline for electrophysiological data was not the focus of this study since a multitude of tools exist, which could be integrated into Lead-OR in the future. However, to demonstrate live processing and visualization of electrophysiological features, for now we included two minimal processing pipelines for MER. (Currently, no pipeline for local field potential recordings is included, but this could be similarly extended given the open-source nature of the tool.).

The first is the signal's normalized root mean square (NRMS) value, which is computed as described in ***Zaidel et al., 2009***. For each step (Microdrive position), a stable part of the recorded data is extracted to compute the RMS on (see Zaidel et al., supplementary material). To obtain a normalized measure, the values along the trajectory are divided by the median of the first five stable steps. To visualize results in space, Lead-OR projects a tube along the trajectory with varying radius and color – both redundantly representing NRMS magnitude. Potentially, in the future, radius and color could be assigned to represent different features that could graphically combine information derived from MER and local field potential signals.

The second processing pipeline is based on spike analysis. This is implemented by running the WaveClus (***Chaure et al., 2018***) automatic pipeline with negative threshold on the recorded files once the drive moves to the next position. Clusters with less than 100 spikes or in which 10% of the inter spike intervals (ISIs) are below 3 ms or in which signal-to-noise ratio (SNR) is less than 1.5 are discarded. SNR is computed as described in ***Joshua et al., 2007*** using the residual method. We assume the recordings capture singe-unit activity (SUA) instead of multiunit activity (MUA), and thus each recording can represent none or one cluster of spikes. One of the reasons behind this assumption is, for example, that changes in amplitude recording from the same unit might be misclassified as different clusters. Spike clusters are represented as fiducials placed in the position they were detected. ***Figure 3*** summarizes the described live-processing setup.

Stimulation module

Intraoperative assessment of stimulation-induced therapeutic as well as side effects can yield important information about electrode placement. For example, electrode placement close to the internal capsule may lead to tonic muscle contractions at low stimulation amplitudes. Often, these thresholds are intraoperatively identified by stimulating at increasing steps until muscle contractions and/or electromyography (EMG) activity are observed. Since Lead-OR already visualizes the patient-specific location of the stimulation sites, volumes of tissue activated (VTA) could be used as seeds for tractography. Fiber analysis was carried out by accessing the logic of the SlicerDMRI module (***Norton et al., 2017***).

Obtaining preoperative diffusion MRI data is not part of clinical practice at all DBS centers. In cases where patient-specific dMRI data is not available, an alternative is to use normative fibers that are defined in template space and warped into patient space (similar to other types of atlas data). This process can at times even come with advantages, for example, the absence of false-positive fibers when using manually curated normative datasets (***Petersen et al., 2019***; for a more thorough discussion, see ***Horn and Fox, 2020***). For the purpose of this article, we will refer to the term tractography as the process to filter and visualize tracts derived from such normative datasets or whole-brain

tractography connectomes (**Reisert et al., 2011**) that intersect with a region of interest (ROI) (in our case, the VTA). The exact same process is possible using patient-specific streamlines but is not demonstrated here.

To estimate the VTA, we use the simplified method proposed by **Dembek et al., 2017**, which defines the radius of a sphere based on stimulation amplitude and pulse width. Varying values from 0.5 to 1.0 were set for the constant k_2 in their formula (see Dembek et al., supplementary material, for the explanation of the parameter). In our present example, a value of ~ 0.8 seemed to yield results that matched the recorded EMG data. Currently, this part of this article should be seen as exploratory as an example of feasibility. Data to validate the approach on a larger number of patients beyond the present case was lacking. Further studies are needed to titrate the k_2 value on a group level and validate the stimulation module of Lead-OR in general.

Patient cohort and surgical procedure

Up to this point, we described the live setup of Lead-OR. We aimed to evaluate the accuracy of this setup by comparing imaging- and electrophysiology-derived markers on a group level. To do so, we retrospectively gathered data from patients who underwent DBS and processed it in a similar fashion as the real-time application. 52 patients (12 females; mean age $= 61 \pm 9$) were retrieved from cases undergoing STN-DBS surgery at Charité – Universitätsmedizin Berlin between 07/2017 and 10/2021. Inclusion was based on having homogeneous data acquisitions consistent with current surgical procedure (i.e., Brainlab planning exports together with corresponding imaging acquisitions and complete microelectrode recording information). **Supplementary file 1** summarizes the inclusion process in the form of a flow chart.

Patients underwent bilateral DBS surgery targeting the STN. Surgery was either performed awake or under general anesthesia. In case of the latter, the depth of narcosis was reduced before MERs to reduce potential effects of anesthetic drugs.

The NeuroOmega System (Alpha Omega Engineering) was used with 2–5 microelectrodes in orthogonal (0°) or rotated (45°) Ben-Gun configuration to acquire MERs. Recordings were carried out from 10 mm above to 4 mm below the target with step sizes between 0.2 mm and 0.5 mm (with some exceptions common to clinical practice). Then, microelectrodes were removed and test stimulations were applied at multiple heights above the target via macroelectrodes on central and alternate trajectories. Neuroprobe Sonus non-shielded microelectrodes (Alpha Omega Engineering) were used as micro-/macroelectrodes. Stimulations were done at increasing amplitude steps of 0.5 mA until identifying permanent side effects. Additionally, therapeutic stimulation effects were evaluated when the surgery was performed in the awake state. Patients who underwent general anesthesia received additional EMG using needle electrodes to evaluate motor unit activity of eight muscles as indicator for the activation of corticobulbar and corticospinal tracts. Finally, based on imaging, electrophysiological, and clinical findings, the surgical team decided upon the optimal depth and trajectory for permanent electrode implantation.

Of the 52 patients included in this study, 4 were discarded based on poor imaging quality and 16 based on poor electrophysiology signals (both determined by visual inspection). Additionally, taking the same considerations, four left and four right hemispheres were also discarded based on a low quality of electrophysiology data. MERs were saved as segments for each distance to the target value. Segments were discarded if they were contaminated by artifacts or when their recording length was less than 4 s. With these considerations, we analyzed a final cohort of 32 patients (56 hemispheres) with a total of 236 trajectories.

Imaging and electrophysiology processing

Pre- and postoperative imaging data were co-registered and normalized using Lead-DBS (**Horn et al., 2019**) followed by visual inspection and, if necessary, refinement using WarpDrive. The definitions of the central trajectories were extracted from stereotactic planning reports and the Ben-Gun configuration from recordings files. We computed the NRMS of all trajectories and resampled them on a linear space with 0.1 mm distance to target resolution. Spike clusters were computed as described above. As mentioned earlier, if more than one cluster was detected in a segment and satisfied the stated conditions, this was still considered an SUA (and represented as one cluster in further analysis).

Using the Lead-DBS pipeline, we carried out brain shift correction using postoperative CT data (***Horn et al., 2019***). This allowed us to quantify the degree of brain shift occurring after surgery based on imaging-derived metrics. For each trajectory, each recording position was displaced using the brain shift correction transform. We took the median of displacements as the amount of brain shift for each trajectory. We will refer to this measure as the imaging-based brain shift estimate in this article (note that it is derived from pre- and postoperative imaging data).

The most recently available clinical stimulation settings were retrieved from all 32 patients (visits ranging from 3 to 44 months after surgery). We reconstructed DBS electrodes based on the standard Lead-DBS pipeline and denoted the coordinate of the active contact (in case of multiple active contacts, their locations were averaged). For a qualitative analysis, we projected this coordinate to the nearest point along the closest trajectory for each electrode.

Each recording segment had its own patient-specific distance to target measure. In order to carry out group analyses, we defined a normalized distance to target. With the nonlinear deformation displacement fields, a link between the location of the trajectory and the ICBM 2009b NLIN ASYM (***Fonov et al., 2009***) ('MNI') space was established. We then took a reference point in each trajectory computed as the nearest point to the STN target coordinates in MNI space from ***Caire et al., 2013***. The normalized distance to the target was defined by aligning the references of all trajectories. The alignment was done by displacing each trajectory by its reference position minus the average displacement from all trajectories (***Figure 5—source code 1***). Furthermore, by using the warp to MNI space we were able to compute the trajectory's distance to the STN and the STN entry and exit sites (henceforth referred to as imaging-defined STN boundaries). To do this, we used the STN as defined by the DISTAL atlas. The main hypothesis from the group analysis was that electrophysiological recordings acquired from within the imaging-defined STN would show higher activity than the ones recorded outside of the STN.

All spike clusters were mapped to the left hemisphere of the MNI space (right hemisphere coordinates were nonlinearly flipped). Then, we created an image of 0.22 mm isotropic resolution where each voxel represented the number of clusters detected divided by the number of segment recordings within 1 mm of the voxel's center. This resulted in a cluster density volume in MNI space (***Figure 5—source code 1***; ***Figure 5—source data 2***).

Additionally, NRMS values and STN distances for each trajectory were transformed with the inverse tangent function resulting in similar distributions of the two. Subsequent cross-correlation of these two signals along each trajectory resulted in a maximum cross-correlation value and the lag (displacement) at which this maximum occurred (***Figure 5—source code 2***).

In the next step, we sorted the trajectories according to their maximum cross-correlation and split the data in half, retaining the trajectories that were in close proximity to the STN and showed electrophysiological activity. We then sorted the top half according to the lag at which the maximum cross-correlation occurred (***Figure 5—source code 2***). We will refer to this lag as the electrophysiology-based brain shift estimate (note that it is derived from preoperative imaging and intraoperative electrophysiology). Hence, in contrast to the imaging-derived brain shift estimate (which required postoperative imaging), this one could be computed during surgery. The electrophysiology-based brain shift measures were compared to the imaging-based brain shift estimates in two ways: first, we contrasted imaging-based brain shift estimates between the low versus high-lag groups using Wilcoxon's signed-rank test. The high-lag group was defined by taking trajectories with lag values above 1 standard deviation of the lags. The low-lag group is composed of the same number of trajectories taken from the data sorted according to the lag. This would analyze whether cases with high electrophysiology-derived estimates indeed had more brain shift based on the imaging-based estimate. Second, we correlated values from the high-lag trajectories (where significant brain shift was estimated based on electrophysiology) with the imaging-derived estimate of brain shift. This would analyze whether the degree of brain shift would correlate between electrophysiology- and imaging-derived estimates.

Results

The main result of this work consists of an integrated software framework that links electrophysiological with imaging-derived data within the same patient-specific coordinate space during surgery. ***Figure 4*** shows the software output for a single-case example including different forms of visualization and an exemplary match between DBS imaging and electrophysiology. Furthermore,

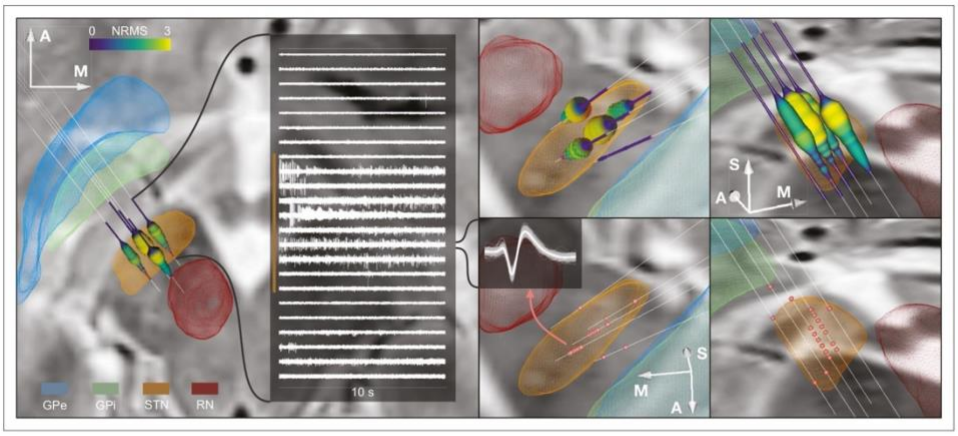

Figure 4. Example case showing trajectories, microelectrode recording (MER) features, and DISTAL atlas volumes mapped to patient space. 10 s recording snippets from one trajectory are displayed. Normalized root mean square (NRMS) activity is represented by a tube with varying diameter and color matching the value. Spike clusters are represented by red point fiducials. GPe: external segment of the globus pallidus; GPi: internal segment of the globus pallidus; STN: subthalamic nucleus; RN: red nucleus.

The online version of this article includes the following video, source data, and figure supplement(s) for figure 4:

Figure supplement 1. Additional ventral intermediate nucleus (VIM) and internal segment of the globus pallidus (GPi) cases.

Figure supplement 2. Additional example cases of subthalamic nucleus-deep brain stimulation (STN-DBS) Lead-OR visualizations.

Figure 4—video 1. General overview of the Lead-OR real-time application.
https://elifesciences.org/articles/72929/figures#fig4video1

Figure 4—video 2. Video showing the program user interface and its use.
https://elifesciences.org/articles/72929/figures#fig4video2

Source data 1. Slicer scene containing the spatial data shown in the ***Figure 4***.

Figure 4—figure supplement 1 shows the application of the tool in a ventral intermediate nucleus (VIM) and GPi example. Finally, for illustrative purposes, we included additionally three STN cases with unusual anatomical configurations in ***Figure 4—figure supplement 2***. ***Figure 4—video 1*** shows the live application of the tool in action, and ***Figure 4—video 2*** shows the user interface and how the platform is setup.

Figure 5 shows the 236 trajectories retrospectively gathered from 32 patients, arranged from left to right based on their distance to the STN and vertically aligned with the normalized distance to target. Electrophysiology traces were plotted with STN entry and exit markers derived from imaging. Comparing the NRMS from the bottom 20% (outside of the STN) to the top 20% revealed an anatomical region with significant differences ($p<0.01$) within the imaging-defined STN boundaries (defined as the median of the top 20% STN boundaries). In other words, the recorded activity from inside this part of the STN was significantly higher than the ones recorded outside of it. Data were compared using nonparametric Wilcoxon's signed-rank test and multiple comparisons were corrected using false discovery rate (FDR) (***Benjamini et al., 2006***).

The cluster density volume in MNI space also showed a general agreement with the imaging-derived STN: when thresholding the volume based on increasing density values, the overlap with the STN region was higher (95% overlap at a 50% cluster density threshold; ***Figure 5***).

With respect to the brain shift analysis, the low-lag and high-lag groups showed a significantly different brain shift distribution (Wilcoxon's signed-rank test $p=0.0076$). Also, correlating the high-lag values (electrophysiology-derived brain shift estimate) with their imaging-derived brain shift estimates showed a significant association ($R = 0.40$, $p=0.016$; ***Figure 5—figure supplement 1***). ***Figure 5—figure supplement 2*** shows an example case illustrating how the imaging-based brain shift-corrected Lead-OR scene presents better correspondence between imaging and MER.

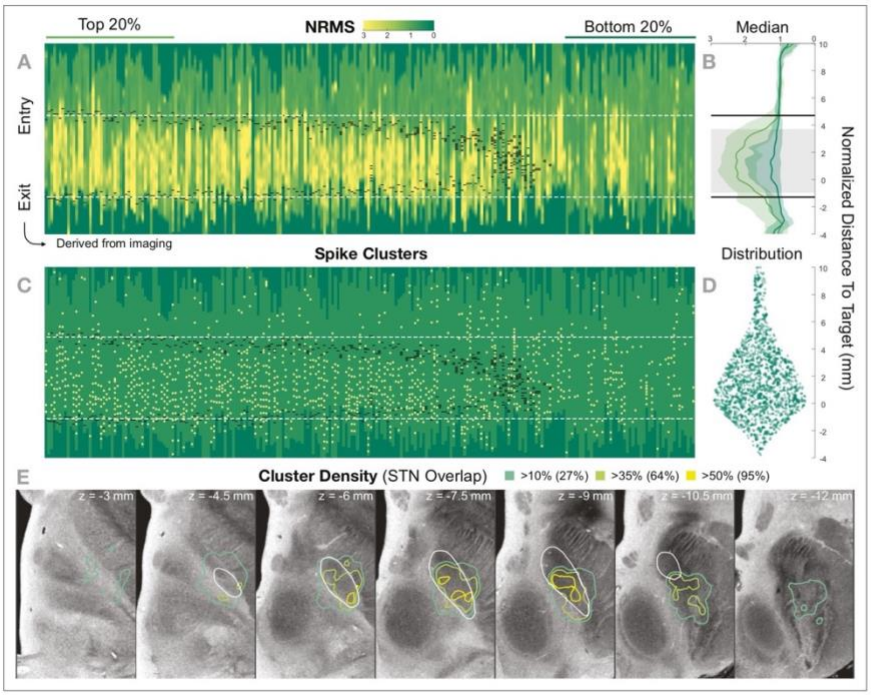

Figure 5. Retrospective group analysis investigating agreement between imaging- and electrophysiology-defined subthalamic nucleus (STN). In (**A**) and (**C**), each trajectory is presented as a column, showing normalized root mean square activity (NRMS) and spike clusters, respectively, with the normalized distance to target denoted on vertical axes. Trajectories are sorted from left to right according to their distance to the STN as defined in the DISTAL atlas (***Ewert et al., 2018***). Dark green values (indicating NRMS of zero) represent no recordings at these sites. Black dashes represent STN entry and exit, and the dashed white line the median entry and exit for the top 20%. (**B**) shows comparisons between bottom and top trajectories, with the gray area representing a significant band (nonparametric Wilcoxon's signed-rank test $p<0.01$ with false discovery rate [FDR] correction), which resides within the STN. The plots show median, 0.25 and 0.75 quantiles. (**D**) shows the overall distribution of spike clusters. (**E**) shows isosurfaces of a volume where each voxel contains the number of clusters detected divided by the number of recordings carried out within 1 mm distance to the location (cluster density). The legend shows the percentage of the volume overlap with the STN at different thresholds. The 7 T MRI ex vivo human brain template (***Edlow et al., 2019***) is shown as the background image with DISTAL STN outline. Decreasing values on the z-axis traverse from superior to inferior.

The online version of this article includes the following source data, source code, and figure supplement(s) for figure 5:

Source code 1. Uses ***Figure 5—source data 1*** to generate ***Figure 5—source data 2*** and panels A–D.

Source code 2. Uses ***Figure 5—source data 1*** to generate ***Figure 5—figure supplement 1***.

Source data 1. Trajectories data including normalized root mean square (NRMS) traces, subthalamic nucleus (STN) entry-exit positions, spike clusters, brain shift, and distance to STN values.

Source data 2. Cluster density volume shown in Figure 5E.

Figure supplement 1. Brain shift study.

Figure supplement 2. Example case in which the imaging-derived brain shift transform was applied to the Lead-OR scene, post-hoc.

Figure supplement 3. Active contact coordinates overlayed with ***Figure 5A and E***.

In ***Figure 5—figure supplement 3***, we show clinical active contact coordinates with respect to the results of the group analysis as shown in ***Figure 5***. Most of the coordinates rely inside the STN and coincide with high-activity regions as depicted by the microelectrode recordings.

Figure 6 shows an example case using the test stimulation setup with live volume activation tractography and corresponding EMG activity invasively recorded during surgical routine using a needle

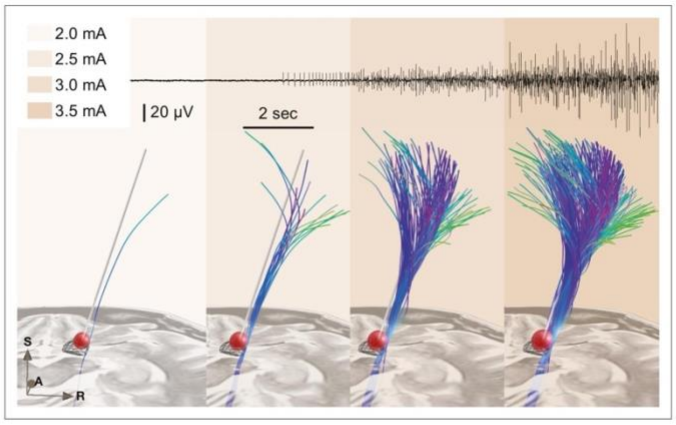

Figure 6. Example of test stimulation setup (also see ***Figure 4—video 1*** for the demonstration of a real-time application). A simplified stimulation volume is modeled based on the applied test stimulation parameters following the approach of ***Dembek et al., 2017***. From a set of predefined fiber tracts representing the internal capsule (without hyperdirect components; ***Petersen et al., 2019***) that were registered to patient space, fibers passing through the volume were visualized in real time. Alternatively, tractograms obtained based on diffusion MRI of the individual patient data or normative connectomes could be used. The top panel shows needle electromyography (EMG) activity that was recorded within clinical routine from the brachioradialis muscle during stimulation in the same patient. Colors represent stimulation amplitude. After a preliminary exploratory analysis of the k_2 parameter from Dembek's formula, a value of 0.8 was used for the shown example.

The online version of this article includes the following source data for figure 6:

Source data 1. Slicer scene containing the spatial data shown in the ***Figure 6***.

electrode inserted into the brachioradialis muscle. We also refer to ***Figure 4—video 1*** for a demonstration of the real-time application of this module.

Discussion

Multiple take-home points can be drawn from this study. First, we established a software pipeline to integrate imaging and electrophysiology results within an interactive real-time application during DBS surgery. The setup interacts with commercial tools for surgical planning and MERs and has the capability to visualize and analyze data in various forms. In the presented group study, the data acquisition conditions were not controlled for, given their retrospective nature. However, the platform can generalize to alternate settings. For example, the number of trajectories used can be set from 1 to 5, without compromising its execution. With respect to hardware settings, while currently a fixed set of interfaces to commercial tools is available, the open-source nature of the software will allow integration of links to other devices. Furthermore, although we present the tool and analysis made with STN cases, it could also be applied to other DBS targets. As illustrative examples, we refer to ***Figure 4—figure supplement 1*** to see Lead-OR visualizations for a VIM and GPi case. Second, atlas data from ultra-high-resolution resources may be integrated into the tool. For instance, whole-brain histological atlases, such as the BigBrain dataset (***Amunts et al., 2013***) or stereotactic 3D atlases, such as the DISTAL (***Ewert et al., 2018***) or Human Thalamus Atlas (***Ilinsky et al., 2018***) could be integrated. In a way, these atlases would fill the gap of commonly used histological reference atlases available in book format, such as the Schaltenbrandt-Wahren (***Schaltenbrand et al., 1977***) or Talairach atlases (***Rey et al., 1988***). While these book resources have been and still are invaluable to the field, they lack the possibility to be deformed into native patient space and to be digitally represented in direct synopsis with patient imaging and electrophysiology. Instead, whole-brain resources will grow in number, resolution, and quality in the foreseeable future (***Horn, 2019***; ***Krauss et al., 2021***; ***Sui et al., 2020***; ***Vedam-Mai et al., 2021***). Similarly to anatomical atlas resources, optimal target definitions

('sweet spots') or even connectomic/tract-based target definitions could one day be integrated to guide DBS surgery – after proper and prospective validation of such datasets and applied methods (***Dembek et al., 2019***; ***Boutet et al., 2021***; ***Elias et al., 2021***). On the hardware side, other possible integrations to the platform in the future include the use of intraoperative imaging such as CT or X-ray acquired for final verification of electrode placement. Data from these acquisitions could potentially be integrated to further enhance visualizations provided by Lead-OR.

The tools, methods, and software described here are not approved by any regulatory authorities and are not intended to assist in making clinical decisions. Rather, we present them for use for purely research-driven purposes under proper IRB approval in study contexts. The tool should be seen as a data visualization tool that could potentially save researchers time by showing data from multiple sources in direct synopsis to one another. As such, it may be powerful to further explore the interplay between electrophysiology and imaging, validate biophysical models, and better characterize patient-specific data.

We see special value in integrating MER-derived measures to the anatomical realm and in the integration with imaging findings. Our aim was to produce a set of use cases each of which could open larger windows of opportunities for upcoming studies. For instance, we included two MER processing pipelines in this study, which have previously been studied in different publications (***Koirala et al., 2020***; ***Boëx et al., 2018***; ***Zaidel et al., 2009***). The reason for their adoption was mostly demonstrative, and we do not claim for them to be the best/only choices when it comes to studying STN activity. Future work involves analyzing differences in these and similar processing pipelines to derive a better understanding of MER physiology. Given the open-source nature of this project, it will be feasible to extend usability and incorporate complementary approaches. Lead-OR should be seen as a satellite application to existing intraoperative electrophysiology software tools, not an attempt to replace them. The aim of our application is to augment these existing tools by a projection of recorded signals to anatomical space. It is intended to run in parallel to existing software (either on a secondary machine or on the same computer). Hence, thorough inspection and analysis of electrophysiological signals will remain unchanged for users of existing software, while our tool could hopefully add additional insights into the anatomical origins of recorded signals.

In a similar vein, we see larger potential in the field of activation tractography by studying stimulation spread across brain tissue with biophysical models that could range around varying degrees of complexity (***Butenko et al., 2020***; ***Gunalan et al., 2017***; ***Howell et al., 2019***; ***Noecker et al., 2021***). Differences in connectomes (***Horn and Blankenburg, 2016***) vs. pathway atlases (***Petersen et al., 2019***; ***Alho et al., 2019***; ***Middlebrooks et al., 2020***) vs. individual tractography (***Akram et al., 2017***) acquired in the specific patient could be investigated directly within the operation theater. We foresee that such studies could lead to a better understanding of the mechanism of action of DBS. This study for now showcases this application of visualizing test stimulations in limited and anecdotical form (also see ***Figure 4—video 1***), warranting further investigation and validation.

Finally, we see large potential in the use and further aggregation of ultra-high-resolution atlas data. Already, such datasets have been emerging and incorporated into DBS applications (***Edlow et al., 2019***; ***Horn et al., 2017***). However, we foresee additional datasets that may revolutionize our definition of anatomy and brain connectivity in the future. For instance, the Jülich group has announced an upcoming version of the BigBrain dataset (***Figure 7***, ***Figure 4—video 1***) that will be available in 1 µm resolution (***Horn, 2021***). A recent normative diffusion-MRI connectome available in 760 µm resolution was based on a 9-hr-long scan of a living human brain (***Wang et al., 2021***). Similarly, a structural brain template of the human brain available in 100 µm resolution was acquired by scanning a postmortem brain over 100 hr at $7T$ (***Figure 7***; ***Edlow et al., 2019***). A recently published pathway atlas of the basal ganglia used expert knowledge and insights from animal studies to create the most realistic set of subcortical fibers available to date (***Petersen et al., 2019***). Similar applications involve histological mesh tractography – a novel technique to create accurate tract representations based on histological data (***Alho et al., 2021***) or expert-curated sets of fiber bundles created by tractography on diffusion MRI data from 1000 subjects (***Middlebrooks et al., 2020***). We foresee great use of such resources if the process of registering them to patient space is truly accurate. The WarpDrive method presented here could embody a missing link in the evolution of making co-registration methodology as precise as possible – with specific focus on regions of particular interest (such as the DBS target zone in our application). For instance, if our aim was to overlay the BigBrain atlas to support our anatomical

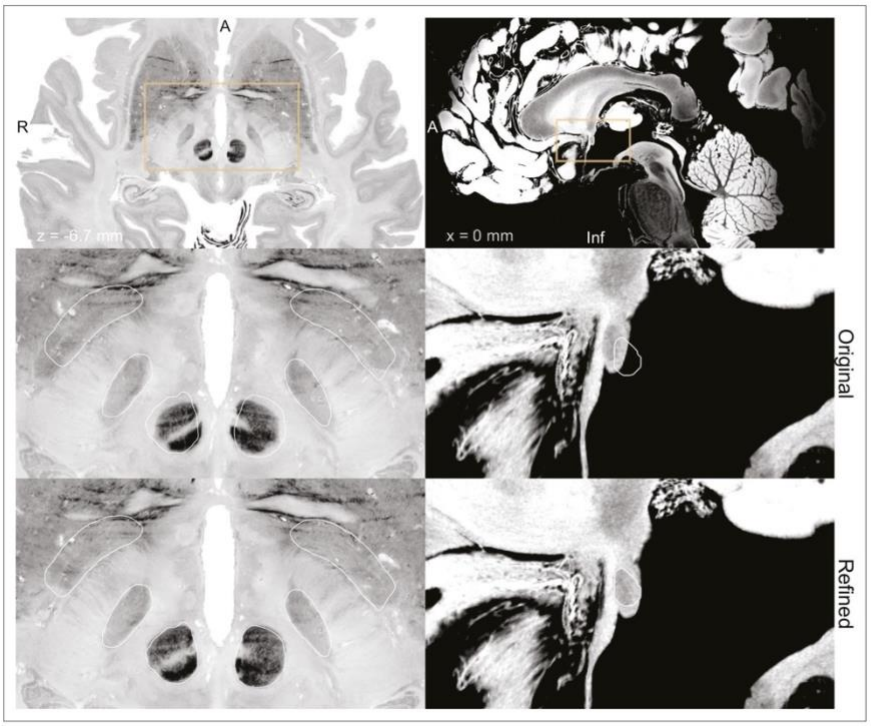

Figure 7. BigBrain (***Amunts et al., 2013***; ***Xiao et al., 2019***) (left) and 7 T MRI ex vivo human brain template (***Edlow et al., 2019***) (right) are two high-resolution (100 µm isotropic) imaging resources that can be used from Lead-DBS and Lead-OR. The middle panel shows a closeup in a plane using the original transformation to MNI space (Xiao et al. in the case of BigBrain) with white outlines of DISTAL atlas (***Ewert et al., 2018***) (left) and anterior commissure from ***Neudorfer et al., 2020*** (right). The bottom panel shows the same slice, but using a refined transformation using Lead-DBS and WarpDrive. The refined transformation files can be found in the supplementary data repository (***Oxenford, 2022a***).

knowledge within and around the STN, it is of crucial importance that the registration between atlas and patient imaging of the STN area is meticulously precise. Instead, registration accuracy of, for example, the parietal lobe will be of lesser importance in this particular scenario. WarpDrive gives the user the necessary toolkit to realize highly precise warps, while focusing on specific ROIs (***Figure 7***, ***Figure 2—video 1***).

Our results demonstrate general agreement between imaging and electrophysiology data on a group level. The recordings throughout the trajectories present a region with higher activity coinciding with the imaging-based STN. However, as can be seen in ***Figure 5***, the agreement is not 100%. Namely, we can observe the presence of activity and high neuronal density in some locations outside of our image-derived model of the STN and vice versa (we observe no activity within voxels that form part of the STN). This emphasizes the possibility of a lack of congruence between preoperative imaging and intraoperative electrophysiological delineation of the STN. Some of these discrepancies could be explained physiologically, for example, seeing activity from regions other than the STN (i.e., thalamic recordings that may be encountered dorsal to the STN or recordings from substantia nigra ventrally). However, true mismatch of the two sources of information (imaging and electrophysiology) *in some cases* is indeed something we would *expect*. Namely, we should not forget that the tool is entirely designed to facilitate integration and visualization of *different* sources of information in parallel. If both would perfectly agree in each single case, there would be no need to acquire MER data in the first place. In our brain shift analysis, we could demonstrate that some of these discrepancies are

associated with the occurrence of brain shift. This presented analysis could be considered a first of its kind attempt to infer brain shift during surgery using a combination of preoperative MRI and intraoperative MER. Specifically, the cross-correlation-derived features may be used as indicators (provided by the program) to quantify discrepancies between MER and imaging data in a real-time setting. This analysis can be further elaborated upon and integrated into future iterations of the platform.

Limitations

Other explanations for disagreement between imaging and electrophysiological data will directly inform limitations that apply to this study. The occurrence of brain shift could be seen as a limitation but also as a feature of our approach (see above). However, true limitations may arise from imprecisions of the imaging pipeline itself. Although a dedicated multispectral imaging pipeline was applied (in the form of Lead-DBS software), which has shown to create meaningful models of DBS in various studies, there will always be a certain degree of imprecision that is unavoidable when using imaging to segment subcortical nuclei. Here, we aimed to further minimize this imprecision by introducing the WarpDrive tool. However, a downside of this tool could be seen in the fact that it involves manual and observer-dependent steps. Detailed anatomical knowledge and optimal imaging quality are needed to achieve maximal registration accuracy. Ideally, multispectral sets of preoperative images that include specialized sequences optimized for the basal ganglia should be used (***Krauss et al., 2021***). Use of ultra-high-field (i.e., 7 *T*) imaging could represent a useful alternative (***Forstmann et al., 2017***), but in this case danger could arise from increased distortion artifacts exactly and especially in the center of the brain (***Neumann et al., 2015***). Hence, as in the procedure of DBS surgery itself, optimal imaging data quality and meticulous use of tools, as well as optimal levels of methodological insights, are needed to assure safe and successful applications.

Finally, the MER analysis also comes with limitations. First, as the data was collected in retrospective fashion, durations of recordings and distances in recording steps when advancing towards the target were not exactly consistent throughout the whole dataset. Second, cardioballistic artifacts, as well as gradual displacement of brain tissue leading to attenuation of spike amplitudes, are recognized problems when applying spike-sorting algorithms in general. Moreover, anesthesia and wakefulness of patients have an impact on the recordable neurophysiological activity patterns and should be considered when making assumptions about the relationship between neuroanatomy and neurophysiology. While here patients were awake in general, this followed periods of anesthesia (following the clinical protocol established at our center). This leads to a nonuniform quality of the recordings that may then present challenges in their interpretation and processing via automatic algorithms. However, we operate in an experienced high-volume DBS center where surgical decisions are made based on the data used here. In other words, signal quality was sufficient for expert-based decision-making. In the future, additional automatic EEG and EMG activity analysis could further augment the validity of the approach. In general, however, the main aim of this article was to demonstrate the use and feasibility of the tool, while dedicated analyses investigating specific neuroscientific questions should take aforementioned nuances into consideration further.

Conclusion

We presented a method and open-source software tool to visualize results derived from MERs in anatomical space, together with information derived from patient-specific MRI data, as well as high-resolution atlas resources during DBS surgery. We demonstrated general agreement between imaging and electrophysiology-derived measures, as well as examples of unavoidable discrepancy between the two modalities. The tool has potential to empower scientific studies investigating several topics outlined in our discussion, as well as high potential for clinical translation and represents a first step to help integrate information across sources within two- and three-dimensional visualization scenes. While the software is not certified and intended for scientific use under IRB approval only, subsequent steps will involve improving and extending the different components of the software to achieve a reliable multimodal patient-specific navigator capable of assisting clinical decision-making.

Data availability

All processed data and code needed to reproduce the main findings of the study are made openly available in deidentified form (see figure legends). This can be found in https://github.com/simonoxen/

Lead-OR_Supplementary, (copy archived at swh:1:rev:c7b8661f0587db992e7eba978d61da8cd7cdc88b; ***Oxenford, 2022a***) and attached to the publication. Due to data privacy regulations of patient data, raw data cannot be publicly shared. Upon reasonable request to the corresponding author, data can be made available after setting up a data-sharing agreement between our host institution (Charité – Universitätsmedizin Berlin) and the inquiring party. All codes used to analyze the dataset are available within Lead-DBS/-OR software (https://github.com/netstim/leaddbs [***Network Stimulation Laboratory, 2022***]; https://github.com/netstim/SlicerNetstim [***Oxenford, 2022b***]).

Acknowledgements

We thank Alaa Hanna from Alpha Omega Engineering for methodological support in interfacing with the NeuroOmega SDK. While the present software implementation works with two commercial products for surgical planning and the intraoperative procedure, the choices of these systems were arbitrary (defined by what was present at our center) and do not mean any form of endorsement whatsoever. No industry funding was received to carry out this study. Part of this study was presented and worked on during the 35th NA-MIC Project Week (Kapur et al., 2016). We would like to thank the NA-MIC community, especially Dr. Andras Lasso and Dr. Steve Pieper for the help and discussions on 3D Slicer modules implementation. AH was supported by the German Research Foundation (Deutsche Forschungsgemeinschaft, Emmy Noether Stipend 410169619 and 424778381 – TRR 295), Deutsches Zentrum für Luft- und Raumfahrt (DynaSti grant within the EU Joint Programme Neurodegenerative Disease Research, JPND), the National Institutes of Health (2R01 MH113929), as well as the Foundation for OCD Research (FFOR). AH is participant in the BIH-Charité Clinician Scientist Program funded by the Charité – Universitätsmedizin Berlin and the Berlin Institute of Health. WJN was supported by Bundesministerium für Bildung und Forschung (BMBF) (Project iDBS FKZ01GQ1802), Deutsche Forschungsgemeinschaft (DFG) (Project ID 424778371 – TRR 295), Hertie Foundation (Project BGPlasticity), and Berlin Institute of Health (Project SPOKES).

Additional information

Competing interests

Andrea Kühn: Reports personal fees from Medtronic, Boston Scientific, Abbott, Teva, Ipsen and Stadapharm, all outside the submitted work. Andreas Horn: Reports lecture fee for Boston Scientific outside the submitted work. The other authors declare that no competing interests exist.

Funding

Funder	Grant reference number	Author
Deutsche Forschungsgemeinschaft	Emmy Noether Stipend 410169619	Andreas Horn
Deutsche Forschungsgemeinschaft	Project ID 424778371	Andreas Horn Wolf-Julian Neumann
Bundesministerium für Bildung und Forschung	Project iDBS FKZ01GQ1802	Wolf-Julian Neumann
Deutsches Zentrum für Luft- und Raumfahrt	DynaSti grant within the EU Joint Programme Neurodegenerative Disease Research JPND	Andreas Horn
National Institutes of Health	2R01 MH113929	Andreas Horn

The funders had no role in study design, data collection and interpretation, or the decision to submit the work for publication.

Author contributions

Simón Oxenford, Conceptualization, Data curation, Formal analysis, Investigation, Methodology, Software, Visualization, Writing – original draft, Writing – review and editing; Jan Roediger,

Conceptualization, Data curation, Formal analysis, Methodology, Writing – original draft, Writing – review and editing; Clemens Neudorfer, Conceptualization, Investigation, Methodology, Writing – review and editing; Luka Milosevic, Conceptualization, Formal analysis, Methodology, Writing – review and editing; Christopher Güttler, Methodology, Writing – review and editing; Philipp Spindler, Data curation, Methodology, Writing – review and editing; Peter Vajkoczy, Wolf-Julian Neumann, Andrea Kühn, Supervision, Writing – review and editing; Andreas Horn, Conceptualization, Formal analysis, Funding acquisition, Investigation, Methodology, Project administration, Software, Supervision, Visualization, Writing – original draft, Writing – review and editing

Author ORCIDs
Simón Oxenford http://orcid.org/0000-0003-2989-3861
Jan Roediger http://orcid.org/0000-0003-2814-3532
Luka Milosevic http://orcid.org/0000-0002-4051-5397
Wolf-Julian Neumann http://orcid.org/0000-0002-6758-9708
Andreas Horn http://orcid.org/0000-0002-0695-6025

Ethics
The collection and analysis of all patient data used for this article was approved by the Local Ethics committee of Charité - Universitätsmedizin Berlin (master vote EA2/145/21). All data were analyzed retrospectively and obtained in deidentified from Medical Records of Charité. Hence, following local guidelines in Berlin/Brandenburg as well as NIH guidelines for human subjects research, no explicit patient consent to analyze and publish was obtained/necessary.

Decision letter and Author response
Decision letter https://doi.org/10.7554/eLife.72929.sa1
Author response https://doi.org/10.7554/eLife.72929.sa2

Additional files

Supplementary files
- Transparent reporting form
- Supplementary file 1. Inclusion flow chart.
- Reporting standard 1. STROBE checklist.

Data availability
All processed data and code needed to reproducemain findings of the study aremade openly available in de-identified form (see figure legends). This can be found in https://github.com/simonoxen/Lead-OR_Supplementary (copy archived at swh:1:rev:c7b8661f0587db992e7eba978d61da8cd7cdc88b). Due to data privacy regulations of patient data, raw data cannot be publicly shared. Upon reasonable request to the corresponding author, data can be made available after setting up a data sharing agreement between our host institution (Charité - Universitätsmedizin Berlin) and the inquiring party. All code used to analyze the dataset is available within Lead-DBS /-OR software (https://github.com/netstim/leaddbs; https://github.com/netstim/SlicerNetstim(copy archived at swh:1:rev:2439c1e117af9027802ba48b67530a0af189c6fe)).

References

Akram H, Sotiropoulos SN, Jbabdi S, Georgiev D, Mahlknecht P, Hyam J, Foltynie T, Limousin P, De Vita E, Jahanshahi M, Hariz M, Ashburner J, Behrens T, Zrinzo L. 2017. Subthalamic deep brain stimulation sweet spots and hyperdirect cortical connectivity in Parkinson's disease. *NeuroImage* **158**:332–345. DOI: https://doi.org/10.1016/j.neuroimage.2017.07.012, PMID: 28711737

Al-Fatly B, Ewert S, Kübler D, Kroneberg D, Horn A, Kühn AA. 2019. Connectivity profile of thalamic deep brain stimulation to effectively treat essential tremor. *Brain: A Journal of Neurology* **142**:3086–3098. DOI: https://doi.org/10.1093/brain/awz236, PMID: 31377766

Alho E, Alho A, Horn A, Martin M, Edlow BL, Fischl B, Nagy J, Fonoff ET, Hamani C, Heinsen H. 2019. The Ansa Subthalamica: A Neglected Fiber Tract. *Movement Disorders* **35**:75–80. DOI: https://doi.org/10.1002/mds.27901, PMID: 31758733

Alho E, Fonoff ET, Di Lorenzo Alho AT, Nagy J, Heinsen H. 2021. Use of computational fluid dynamics for 3D fiber tract visualization on human high-thickness histological slices: histological mesh tractography. *Brain Structure and Function* **226**:323–333. DOI: https://doi.org/10.1007/s00429-020-02187-3, PMID: 33389040

Amunts K, Lepage C, Borgeat L, Mohlberg H, Dickscheid T, Rousseau ME, Bludau S, Bazin PL, Lewis LB, Oros-Peusquens AM, Shah NJ, Lippert T, Zilles K, Evans AC. 2013. BigBrain: An Ultrahigh-Resolution 3D Human Brain Model. *Science (New York, N.Y.)* **340**:1472–1475. DOI: https://doi.org/10.1126/science.1235381

Avants BB, Epstein CL, Grossman M, Gee JC. 2008. Symmetric diffeomorphic image registration with cross-correlation: evaluating automated labeling of elderly and neurodegenerative brain. *Medical Image Analysis* **12**:26–41. DOI: https://doi.org/10.1016/j.media.2007.06.004, PMID: 17659998

Aviles-Olmos I, Kefalopoulou Z, Tripoliti E, Candelario J, Akram H, Martinez-Torres I, Jahanshahi M, Foltynie T, Hariz M, Zrinzo L, Limousin P. 2014. Long-term outcome of subthalamic nucleus deep brain stimulation for Parkinson's disease using an MRI-guided and MRI-verified approach. *Journal of Neurology, Neurosurgery, and Psychiatry* **85**:1419–1425. DOI: https://doi.org/10.1136/jnnp-2013-306907, PMID: 24790212

Benazzouz A, Breit S, Koudsie A, Pollak P, Krack P, Benabid AL. 2002. Intraoperative microrecordings of the subthalamic nucleus in Parkinson's disease. *Movement Disorders* **17 Suppl 3**:S145–S149. DOI: https://doi.org/10.1002/mds.10156, PMID: 11948769

Benjamini Y, Krieger AM, Yekutieli D. 2006. Adaptive linear step-up procedures that control the false discovery rate. *Biometrika* **93**:491–507. DOI: https://doi.org/10.1093/biomet/93.3.491

Boëx C, Tyrand R, Horvath J, Fleury V, Sadri S, Corniola M, Burkhard PR, Momjian S. 2018. What Is the Best Electrophysiologic Marker of the Outcome of Subthalamic Nucleus Stimulation in Parkinson Disease? *World Neurosurgery* **120**:e1217–e1224. DOI: https://doi.org/10.1016/j.wneu.2018.09.047, PMID: 30240865

Boutet A, Germann J, Gwun D, Loh A, Elias GJB, Neudorfer C, Paff M, Horn A, Kuhn AA, Munhoz RP, Kalia SK, Hodaie M, Kucharczyk W, Fasano A, Lozano AM. 2021. Sign-specific stimulation "hot" and "cold" spots in Parkinson's disease validated with machine learning. *Brain Communications* **3**:fcab027. DOI: https://doi.org/10.1093/braincomms/fcab027, PMID: 33870190

Butenko K, Bahls C, Schröder M, Köhling R, van Rienen U. 2020. OSS-DBS: Open-source simulation platform for deep brain stimulation with a comprehensive automated modeling. *PLOS Computational Biology* **16**:e1008023. DOI: https://doi.org/10.1371/journal.pcbi.1008023, PMID: 32628719

Caire F, Ranoux D, Guehl D, Burbaud P, Cuny E. 2013. A systematic review of studies on anatomical position of electrode contacts used for chronic subthalamic stimulation in Parkinson's disease. *Acta Neurochirurgica* **155**:1647–1654; . DOI: https://doi.org/10.1007/s00701-013-1782-1, PMID: 23775325

Chaure FJ, Rey HG, Quian Quiroga R. 2018. A novel and fully automatic spike-sorting implementation with variable number of features. *Journal of Neurophysiology* **120**:1859–1871. DOI: https://doi.org/10.1152/jn.00339.2018, PMID: 29995603

Dembek TA, Barbe MT, Åström M, Hoevels M, Visser-Vandewalle V, Fink GR, Timmermann L. 2017. Probabilistic mapping of deep brain stimulation effects in essential tremor. *NeuroImage. Clinical* **13**:164–173. DOI: https://doi.org/10.1016/j.nicl.2016.11.019, PMID: 27981031

Dembek TA, Roediger J, Horn A, Reker P, Oehrn C, Dafsari HS, Li N, Kühn AA, Fink GR, Visser-Vandewalle V, Barbe MT, Timmermann L. 2019. Probabilistic sweet spots predict motor outcome for deep brain stimulation in Parkinson disease. *Annals of Neurology* **86**:527–538. DOI: https://doi.org/10.1002/ana.25567, PMID: 31376171

Edlow BL, Mareyam A, Horn A, Polimeni JR, Witzel T, Tisdall MD, Augustinack JC, Stockmann JP, Diamond BR, Stevens A, Tirrell LS, Folkerth RD, Wald LL, Fischl B, van der Kouwe A. 2019. 7 Tesla MRI of the ex vivo human brain at 100 micron resolution. *Scientific Data* **6**:244. DOI: https://doi.org/10.1038/s41597-019-0254-8, PMID: 31666530

Elias GJB, Boutet A, Joel SE, Germann J, Gwun D, Neudorfer C, Gramer RM, Algarni M, Paramanandam V, Prasad S, Beyn ME, Horn A, Madhavan R, Ranjan M, Lozano CS, Kühn AA, Ashe J, Kucharczyk W, Munhoz RP, Giacobbe P, et al. 2021. Probabilistic Mapping of Deep Brain Stimulation: Insights from 15 Years of Therapy. *Annals of Neurology* **89**:426–443. DOI: https://doi.org/10.1002/ana.25975, PMID: 33252146

Ewert S, Plettig P, Li N, Chakravarty MM, Collins DL, Herrington TM, Kühn AA, Horn A. 2018. Toward defining deep brain stimulation targets in MNI space: A subcortical atlas based on multimodal MRI, histology and structural connectivity. *NeuroImage* **170**:271–282. DOI: https://doi.org/10.1016/j.neuroimage.2017.05.015, PMID: 28536045

Ewert S., Horn A, Finkel F, Li N, Kühn AA, Herrington TM. 2019. Optimization and comparative evaluation of nonlinear deformation algorithms for atlas-based segmentation of DBS target nuclei. *NeuroImage* **184**:586–598. DOI: https://doi.org/10.1016/j.neuroimage.2018.09.061, PMID: 30267856

Fedorov A, Beichel R, Kalpathy-Cramer J, Finet J, Fillion-Robin JC, Pujol S, Bauer C, Jennings D, Fennessy F, Sonka M, Buatti J, Aylward S, Miller JV, Pieper S, Kikinis R. 2012. 3D Slicer as an image computing platform for the Quantitative Imaging Network. *Magnetic Resonance Imaging* **30**:1323–1341. DOI: https://doi.org/10.1016/j.mri.2012.05.001, PMID: 22770690

Fonov VS, Evans AC, McKinstry RC, Almli CR, Collins DL. 2009. Unbiased nonlinear average age-appropriate brain templates from birth to adulthood. *NeuroImage* **47**:S102. DOI: https://doi.org/10.1016/S1053-8119(09)70884-5

Forstmann BU, Isaacs BR, Temel Y. 2017. Ultra High Field MRI-Guided Deep Brain Stimulation. *Trends in Biotechnology* **35**:904–907. DOI: https://doi.org/10.1016/j.tibtech.2017.06.010, PMID: 28942267

Gunalan K, Chaturvedi A, Howell B, Duchin Y, Lempka SF, Patriat R, Sapiro G, Harel N, McIntyre CC. 2017. Creating and parameterizing patient-specific deep brain stimulation pathway-activation models using the hyperdirect pathway as an example. *PLOS ONE* **12**:e0176132. DOI: https://doi.org/10.1371/journal.pone.0176132, PMID: 28441410

Halpern CH, Danish SF, Baltuch GH, Jaggi JL. 2008. Brain shift during deep brain stimulation surgery for Parkinson's disease. *Stereotactic and Functional Neurosurgery* **86**:37–43. DOI: https://doi.org/10.1159/000108587, PMID: 17881887

Horn A, Kühn AA. 2015. Lead-DBS: A toolbox for deep brain stimulation electrode localizations and visualizations. *NeuroImage* **107**:127–135. DOI: https://doi.org/10.1016/j.neuroimage.2014.12.002, PMID: 25498389

Horn A, Blankenburg F. 2016. Toward a standardized structural-functional group connectome in MNI space. *NeuroImage* **124**:310–322. DOI: https://doi.org/10.1016/j.neuroimage.2015.08.048, PMID: 26327244

Horn A, Kühn AA, Merkl A, Shih L, Alterman R, Fox M. 2017. Probabilistic conversion of neurosurgical DBS electrode coordinates into MNI space. *NeuroImage* **150**:395–404. DOI: https://doi.org/10.1016/j.neuroimage.2017.02.004, PMID: 28163141

Horn A. 2019. The impact of modern-day neuroimaging on the field of deep brain stimulation. *Current Opinion in Neurology* **32**:511–520. DOI: https://doi.org/10.1097/WCO.0000000000000679, PMID: 30844863

Horn A, Li N, Dembek TA, Kappel A, Boulay C, Ewert S, Tietze A, Husch A, Perera T, Neumann WJ, Reisert M, Si H, Oostenveld R, Rorden C, Yeh FC, Fang Q, Herrington TM, Vorwerk J, Kühn AA. 2019. Lead-DBS v2: Towards a comprehensive pipeline for deep brain stimulation imaging. *NeuroImage* **184**:293–316. DOI: https://doi.org/10.1016/j.neuroimage.2018.08.068, PMID: 30179717

Horn A, Fox MD. 2020. Opportunities of connectomic neuromodulation. *NeuroImage* **221**:117180. DOI: https://doi.org/10.1016/j.neuroimage.2020.117180, PMID: 32702488

Horn A. 2021. 11: Katrin Amunts – A modern take on human brain anatomy and its relevance to DBS. Figshare. https://figshare.com/articles/media/_11_Katrin_Amunts_A_modern_take_on_human_brain_anatomy_and_its_relevance_to_DBS/14501976/1

Howell B, Gunalan K, McIntyre CC. 2019. A Driving-Force Predictor for Estimating Pathway Activation in Patient-Specific Models of Deep Brain Stimulation. *Neuromodulation* **22**:403–415. DOI: https://doi.org/10.1111/ner.12929, PMID: 30775834

Ilinsky I, Horn A, Paul-Gilloteaux P, Gressens P, Verney C, Kultas-Ilinsky K. 2018. Human Motor Thalamus Reconstructed in 3D from Continuous Sagittal Sections with Identified Subcortical Afferent Territories. *ENeuro* **5**:0060-18. DOI: https://doi.org/10.1523/ENEURO.0060-18.2018, PMID: 30023427

Joshua M, Elias S, Levine O, Bergman H. 2007. Quantifying the isolation quality of extracellularly recorded action potentials. *Journal of Neuroscience Methods* **163**:267–282. DOI: https://doi.org/10.1016/j.jneumeth.2007.03.012, PMID: 17477972

Kapur T, Pieper S, Fedorov A, Fillion-Robin J-C, Halle M, O'Donnell L, Lasso A, Ungi T, Pinter C, Finet J, Pujol S, Jagadeesan J, Tokuda J, Norton I, Estepar RSJ, Gering D, Aerts HJWL, Jakab M, Hata N, Ibanez L, et al. 2016. Increasing the impact of medical image computing using community-based open-access hackathons: The NA-MIC and 3D Slicer experience. *Medical Image Analysis* **33**:176–180. DOI: https://doi.org/10.1016/j.media.2016.06.035, PMID: 27498015

Koirala N, Serrano L, Paschen S, Falk D, Anwar AR, Kuravi P, Deuschl G, Groppa S, Muthuraman M. 2020. Mapping of subthalamic nucleus using microelectrode recordings during deep brain stimulation. *Scientific Reports* **10**:19241. DOI: https://doi.org/10.1038/s41598-020-74196-5, PMID: 33159098

Krauss JK, Lipsman N, Aziz T, Boutet A, Brown P, Chang JW, Davidson B, Grill WM, Hariz MI, Horn A, Schulder M, Mammis A, Tass PA, Volkmann J, Lozano AM. 2021. Technology of deep brain stimulation: current status and future directions. *Nature Reviews. Neurology* **17**:75–87. DOI: https://doi.org/10.1038/s41582-020-00426-z, PMID: 33244188

Krüger M. 2020. Navigated Deep Brain Stimulation Surgery: Evaluating the Combined Use of a Frame-Based Stereotactic System and a Navigation System. *Stereotactic and Functional Neurosurgery* **1**:7.

Li N, Baldermann JC, Kibleur A, Treu S, Akram H, Elias GJB, Boutet A, Lozano AM, Al-Fatly B, Strange B, Barcia JA, Zrinzo L, Joyce E, Chabardes S, Visser-Vandewalle V, Polosan M, Kuhn J, Kühn AA, Horn A. 2020. A unified connectomic target for deep brain stimulation in obsessive-compulsive disorder. *Nature Communications* **11**:3364. DOI: https://doi.org/10.1038/s41467-020-16734-3, PMID: 32620886

Lozano CS, Ranjan M, Boutet A, Xu DS, Kucharczyk W, Fasano A, Lozano AM. 2018. Imaging alone versus microelectrode recording-guided targeting of the STN in patients with Parkinson's disease. *Journal of Neurosurgery* **130**:1–6. DOI: https://doi.org/10.3171/2018.2.JNS172186, PMID: 30074454

Middlebrooks EH, Domingo RA, Vivas-Buitrago T, Okromelidze L, Tsuboi T, Wong JK, Eisinger RS, Almeida L, Burns MR, Horn A, Uitti RJ, Wharen RE, Holanda VM, Grewal SS. 2020. Neuroimaging Advances in Deep Brain Stimulation: Review of Indications, Anatomy, and Brain Connectomics. *AJNR. American Journal of Neuroradiology* **41**:1558–1568. DOI: https://doi.org/10.3174/ajnr.A6693, PMID: 32816768

Network Stimulation Laboratory. 2022. leaddbs. d3b55fd. GitHub. https://github.com/netstim/leaddbs

Neudorfer C, Germann J, Elias GJB, Gramer R, Boutet A, Lozano AM. 2020. A high-resolution in vivo magnetic resonance imaging atlas of the human hypothalamic region. *Scientific Data* **7**:305. DOI: https://doi.org/10.1038/s41597-020-00644-6, PMID: 32934244

Neumann JO, Giese H, Biller A, Nagel AM, Kiening K. 2015. Spatial Distortion in MRI-Guided Stereotactic Procedures: Evaluation in 1.5-, 3- and 7-Tesla MRI Scanners. *Stereotactic and Functional Neurosurgery* **93**:380–386. DOI: https://doi.org/10.1159/000441233, PMID: 26671683

Noecker AM, Frankemolle-Gilbert AM, Howell B, Petersen MV, Beylergil SB, Shaikh AG, McIntyre CC. 2021. StimVision v2: Examples and Applications in Subthalamic Deep Brain Stimulation for Parkinson's Disease. *Neuromodulation* **24**:248–258. DOI: https://doi.org/10.1111/ner.13350, PMID: 33389779

Norton I, Essayed WI, Zhang F, Pujol S, Yarmarkovich A, Golby AJ, Kindlmann G, Wassermann D, Estepar RSJ, Rathi Y, Pieper S, Kikinis R, Johnson HJ, Westin C-F, O'Donnell LJ. 2017. SlicerDMRI: Open Source Diffusion MRI Software for Brain Cancer Research. *Cancer Research* **77**:e101–e103. DOI: https://doi.org/10.1158/0008-5472.CAN-17-0332, PMID: 29092950

Oxenford S. 2022a. Lead-OR_Supplementary. swh:1:rev:c7b8661f0587db992e7eba978d61da8cd7cdc88b. GitHub. https://github.com/simonoxen/Lead-OR_Supplementary

Oxenford S. 2022b. SlicerNetstim. swh:1:rev:2439c1e117af9027802ba48b67530a0af189c6fe. GitHub. https://github.com/netstim/SlicerNetstim

Petersen MV, Mlakar J, Haber SN, Parent M, Smith Y, Strick PL, Griswold MA, McIntyre CC. 2019. Holographic Reconstruction of Axonal Pathways in the Human Brain. *Neuron* **104**:1056-1064.. DOI: https://doi.org/10.1016/j.neuron.2019.09.030, PMID: 31708306

Reisert M, Mader I, Anastasopoulos C, Weigel M, Schnell S, Kiselev V. 2011. Global fiber reconstruction becomes practical. *NeuroImage* **54**:955–962. DOI: https://doi.org/10.1016/j.neuroimage.2010.09.016, PMID: 20854913

Rey M, Dellatolas G, Bancaud J, Talairach J. 1988. Hemispheric lateralization of motor and speech functions after early brain lesion: study of 73 epileptic patients with intracarotid amytal test. *Neuropsychologia* **26**:167–172. DOI: https://doi.org/10.1016/0028-3932(88)90040-1, PMID: 3129671

Santin MD, Didier M, Valabrègue R, Yahia Cherif L, García-Lorenzo D, Loureiro de Sousa P, Bardinet E, Lehéricy S. 2017. Reproducibility of R_2 * and quantitative susceptibility mapping (QSM) reconstruction methods in the basal ganglia of healthy subjects. *NMR in Biomedicine* **30**:3491. DOI: https://doi.org/10.1002/nbm.3491, PMID: 26913373

Schaltenbrand G, Wahren W, Hassler RG. 1977. Atlas for Stereotaxy of the Human Brain. ThiemeStuttgart.

Sharp GC, Li R, Wolfgang J, Chen G, Peroni M, Spadea MF, Mori S, Zhang J, Shackleford J, Kandasamy N. 2010. Plastimatch-an open source software suite for radiotherapy image processing. In Proceedings of the XVI'th International Conference on the Use of Computers in Radiotherapy (ICCR. .

Sudhyadhom A, Haq IU, Foote KD, Okun MS, Bova FJ. 2009. A high resolution and high contrast MRI for differentiation of subcortical structures for DBS targeting: The Fast Gray Matter Acquisition T1 Inversion Recovery (FGATIR. *NeuroImage* **47**:T44–T52. DOI: https://doi.org/10.1016/j.neuroimage.2009.04.018

Sui Y, Tian Y, Ko WKD, Wang Z, Jia F, Horn A, De Ridder D, Choi KS, Bari AA, Wang S, Hamani C, Baker KB, Machado AG, Aziz TZ, Fonoff ET, Kühn AA, Bergman H, Sanger T, Liu H, Haber SN, et al. 2020. Deep Brain Stimulation Initiative: Toward Innovative Technology, New Disease Indications, and Approaches to Current and Future Clinical Challenges in Neuromodulation Therapy. *Frontiers in Neurology* **11**:597451. DOI: https://doi.org/10.3389/fneur.2020.597451, PMID: 33584498

Thompson JA, Oukal S, Bergman H, Ojemann S, Hebb AO, Hanrahan S, Israel Z, Abosch A. 2018. Semi-automated application for estimating subthalamic nucleus boundaries and optimal target selection for deep brain stimulation implantation surgery. *Journal of Neurosurgery* **1**:10. DOI: https://doi.org/10.3171/2017.12.JNS171964

Tourdias T, Saranathan M, Levesque IR, Su J, Rutt BK. 2014. Visualization of intra-thalamic nuclei with optimized white-matter-nulled MPRAGE at 7T. *NeuroImage* **84**:534–545. DOI: https://doi.org/10.1016/j.neuroimage.2013.08.069, PMID: 24018302

Treu S, Strange B, Oxenford S, Neumann WJ, Kühn A, Li N, Horn A. 2020. Deep brain stimulation: Imaging on a group level. *NeuroImage* **219**:117018. DOI: https://doi.org/10.1016/j.neuroimage.2020.117018, PMID: 32505698

Vassal F, Coste J, Derost P, Mendes V, Gabrillargues J, Nuti C, Durif F, Lemaire JJ. 2012. Direct stereotactic targeting of the ventrointermediate nucleus of the thalamus based on anatomic 1.5-T MRI mapping with a white matter attenuated inversion recovery (WAIR) sequence. *Brain Stimulation* **5**:625–633. DOI: https://doi.org/10.1016/j.brs.2011.10.007, PMID: 22405744

Vedam-Mai V, Deisseroth K, Giordano J, Lazaro-Munoz G, Chiong W, Suthana N, Langevin JP, Gill J, Goodman W, Provenza NR, Halpern CH, Shivacharan RS, Cunningham TN, Sheth SA, Pouratian N, Scangos KW, Mayberg HS, Horn A, Johnson KA, Butson CR, et al. 2021. Corrigendum: Proceedings of the Eighth Annual Deep Brain Stimulation Think Tank: Advances in Optogenetics, Ethical Issues Affecting DBS Research, Neuromodulatory Approaches for Depression, Adaptive Neurostimulation, and Emerging DBS Technologies. *Frontiers in Human Neuroscience* **15**:150. DOI: https://doi.org/10.3389/fnhum.2021.765150, PMID: 34658825

Vogel D, Shah A, Coste J, Lemaire JJ, Wårdell K, Hemm S. 2020. Anatomical brain structures normalization for deep brain stimulation in movement disorders. *NeuroImage. Clinical* **27**:102271. DOI: https://doi.org/10.1016/j.nicl.2020.102271, PMID: 32446242

Wang Y, Liu T. 2015. Quantitative susceptibility mapping (QSM): Decoding MRI data for a tissue magnetic biomarker. *Magnetic Resonance in Medicine* **73**:82–101. DOI: https://doi.org/10.1002/mrm.25358, PMID: 25044035

Wang F, Dong Z, Tian Q, Liao C, Fan Q, Hoge WS, Keil B, Polimeni JR, Wald LL, Huang SY, Setsompop K. 2021. In vivo human whole-brain Connectom diffusion MRI dataset at 760 µm isotropic resolution. *Scientific Data* **8**:122. DOI: https://doi.org/10.1038/s41597-021-00904-z, PMID: 33927203

Xiao Y., Fonov V, Chakravarty MM, Beriault S, Al Subaie F, Sadikot A, Pike GB, Bertrand G, Collins DL. 2017. A dataset of multi-contrast population-averaged brain MRI atlases of A Parkinson's disease cohort. *Data in Brief* **12**:370–379. DOI: https://doi.org/10.1016/j.dib.2017.04.013, PMID: 28491942

Xiao Y, Lau JC, Anderson T, DeKraker J, Collins DL, Peters T, Khan AR. 2019. An accurate registration of the BigBrain dataset with the MNI PD25 and ICBM152 atlases. *Scientific Data* **6**:210. DOI: https://doi.org/10.1038/s41597-019-0217-0, PMID: 31624250

Zaidel A, Spivak A, Shpigelman L, Bergman H, Israel Z. 2009. Delimiting subterritories of the human subthalamic nucleus by means of microelectrode recordings and a Hidden Markov Model. *Movement Disorders* **24**:1785–1793. DOI: https://doi.org/10.1002/mds.22674, PMID: 19533755

Zrinzo L, Foltynie T, Limousin P, Hariz MI. 2012. Reducing hemorrhagic complications in functional neurosurgery: A large case series and systematic literature review. *Journal of Neurosurgery* **116**:84–94. DOI: https://doi.org/10.3171/2011.8.JNS101407, PMID: 21905798

Curriculum Vitae

My curriculum vitae does not appear in the electronic version of my paper for reasons of data protection.

Publication list

Horn, A., Reich, M.M., Ewert, S., Li, N., Al-Fatly, B., Lange, F., Roothans, J., Oxenford, S., Horn, I., Paschen, S., Runge, J., Wodarg, F., Witt, K., Nickl, R.C., Wittstock, M., Schneider, G.-H., Mahlknecht, P., Poewe, W., Eisner, W., Helmers, A.-K., Matthies, C., Krauss, J.K., Deuschl, G., Volkmann, J., Kühn, A.A., 2022b. Optimal deep brain stimulation sites and networks for cervical vs. generalized dystonia. Proceedings of the National Academy of Sciences 119, e2114985119. https://doi.org/10.1073/pnas.2114985119. IF: 12.8

Lofredi, R., Auernig, C.-G., Ewert, S., Irmen, F., Steiner, L.A., Scheller, U., van Wijk, B.C.M., Oxenford, S., Kühn, A.A., Horn, A., 2022. Interrater reliability of deep brain stimulation electrode localizations. NeuroImage 262, 119552. https://doi.org/10.1016/j.neuroimage.2022.119552. IF: 7.4

Neudorfer, C., Butenko, K., Oxenford, S., Rajamani, N., Achtzehn, J., Goede, L., Hollunder, B., Ríos, A.S., Hart, L., Tasserie, J., Fernando, K.B., Nguyen, T.A.K., Al-Fatly, B., Vissani, M., Fox, M., Richardson, R.M., van Rienen, U., Kühn, A.A., Husch, A.D., Opri, E., Dembek, T., Li, N., Horn, A., 2023. Lead-DBS v3.0: Mapping Deep Brain Stimulation Effects to Local Anatomy and Global Networks. NeuroImage 119862. https://doi.org/10.1016/j.neuroimage.2023.119862. IF: 7.4

Oxenford, S., Roediger, J., Neudorfer, C., Milosevic, L., Güttler, C., Spindler, P., Vajkoczy, P., Neumann, W.-J., Kühn, A., Horn, A., 2022. Lead-OR: A multimodal platform for deep brain stimulation surgery. eLife 11, e72929. https://doi.org/10.7554/eLife.72929. IF: 8.7

Ríos, A.S., Oxenford, S., Neudorfer, C., Butenko, K., Li, N., Rajamani, N., Boutet, A., Elias, G.J.B., Germann, J., Loh, A., Deeb, W., Wang, F., Setsompop, K., Salvato, B., Almeida, L.B. de, Foote, K.D., Amaral, R., Rosenberg, P.B., Tang-Wai, D.F., Wolk, D.A., Burke, A.D., Salloway, S., Sabbagh, M.N., Chakravarty, M.M., Smith, G.S., Lyketsos, C.G., Okun, M.S., Anderson, W.S., Mari, Z., Ponce, F.A., Lozano, A.M., Horn, A., 2022. Optimal deep brain stimulation sites and networks for stimulation of the fornix in Alzheimer's disease. Nat Commun 13, 7707. https://doi.org/10.1038/s41467-022-34510-3. IF: 17.7

Treu, S., Strange, B., Oxenford, S., Neumann, W.-J., Kühn, A., Li, N., Horn, A., 2020. Deep brain stimulation: Imaging on a group level. NeuroImage 219, 117018. https://doi.org/10.1016/j.neuroimage.2020.117018. IF: 6.5

Wang, Q., Akram, H., Muthuraman, M., Gonzalez-Escamilla, G., Sheth, S.A., Oxenford, S., Yeh, F.-C., Groppa, S., Vanegas-Arroyave, N., Zrinzo, L., Li, N., Kühn, A., Horn, A., 2021. Normative vs. patient-specific brain connectivity in deep brain stimulation. NeuroImage 224, 117307. https://doi.org/10.1016/j.neuroimage.2020.117307. IF: 7.4

Acknowledgments

I would first like thank my supervisor for giving me the opportunity of embarking in this experience; and for guiding me through it. I would also like to thank my fellow lab members, with whom it was a great pleasure to work over the last years. Finally, my greatest gratitude goes to my friends and family—from close and afar they were always present supporting me in this journey.